Ionics
https://doi.org/10.1007/s11581-025-06600-x

RESEARCH

Parameter estimation of proton exchange membrane fuel cell using hybrid grouping biogeography optimization algorithm

Ramesh Kumar[1] · Manish Kumar Singla[2,3] · Muhammed Ali S.A.[4] · Jyoti Gupta[5] · Pradeep Jangir[6,7] · Arpita[8] · El-Sayed M. El-Kenawy[9] · Amal H. Alharbi[10] · Reena Jangid[11,12]

Received: 5 March 2025 / Revised: 8 July 2025 / Accepted: 27 July 2025

Abstract

Proton exchange membrane fuel cells (PEMFCs) are vital for sustainable energy applications due to their efficiency, low emissions, and quiet operation. Accurate optimization of design variables is essential for their performance enhancement, but existing algorithms like WR-BBO, TB-BBO, and HBBOS struggle with issues like slow convergence, local optima entrapment, and parameter sensitivity. The hybrid grouping biogeography-based optimization (HG-BBO) algorithm uses migration and mutation operators for local and global search, respectively. HG-BBO was applied to optimize the design variables of 12 PEMFC stacks: BCS 500 W, Nedstack 600 W PS6, SR-12 W, Horizon H-12, Ballard Mark V, and STD 250 W. Comparative analysis with algorithms such as BBO-M, DE-BBO, Lx-BBO, BHCS, BLPSO, and HBBOS revealed that HG-BBO outperforms them in terms of accuracy, convergence speed, and robustness. The objective function sum of squared error (SSE) for stack voltage is minimized using different algorithms for comparative analysis. Simulation results for *I-V* and *V-P* characteristics aligned closely with experimental data under varying temperature and pressure conditions. These findings highlight HG-BBO's theoretical significance in solving nonlinear optimization problems and its practical utility in enhancing PEMFC design and operational reliability. Future work will focus on real-time optimization, algorithm hybridization, and scaling to larger energy systems, offering a robust tool for advancing PEMFC technology.

Keywords PEMFC · HG-BBO · Design variable optimization · Fuel cell performance · Voltage-current characteristics · Machine learning

Introduction

Declining fossil fuel reserves and the pressing need to mitigate pollution and climate change are driving a global shift towards renewable energy. Fuel cells are a key renewable energy technology, offering high efficiency, durability, and environmental advantages. Their versatility, high power density, rapid start-up, and ability to adapt to fluctuating loads are particularly beneficial. The low operating temperatures and pressures also enhance safety. This adaptability has led to their use in residential, commercial, and industrial sectors, including stationary, portable, and transportation applications [1]. Fuel cells are classified by their electrolyte type, which affects operating temperature, power output, efficiency, and suitable applications. Examples include alkaline, proton exchange membrane (PEM), phosphoric acid, solid oxide, and molten carbonate fuel cells [2, 3]. PEM fuel cells represent a promising clean energy solution, producing electricity from hydrogen and oxygen, with only water as a by-product. However, high catalyst costs hinder their widespread commercialization [4]. Moreover, PEM fuel cells exhibit a variable output voltage that decreases nonlinearly with increasing load due to operational losses. This voltage drop is initially steep due to activation losses, then gradually lessens due to ohmic losses, and finally declines more rapidly at higher loads due to concentration losses [5].

A key focus of PEMFC research is characterizing performance beyond manufacturer specifications and developing highly accurate models of PEMFC voltage–current behavior. This modeling is challenging due to the inherent nonlinearity of PEMFCs [6]. Accurate models are essential for various applications, including performance evaluation, optimal control strategies, realistic simulations, and maximizing power output through techniques like maximum power point tracking [7–10]. To address this complexity, researchers have developed various models,

Extended author information available on the last page of the article

Published online: 08 September 2025

broadly classified as mechanistic, empirical, and semiempirical (such as Amphlett's model) [11–14]. The semiempirical PEMFC model is particularly valuable because it can accurately represent output characteristics by incorporating key operational parameters like fluid pressure, cell temperature, and airflow rate [15]. PEMFC parameter identification has been extensively studied, with established techniques broadly categorized as traditional methods and metaheuristic algorithms [16–18]. Traditional techniques, such as gradient-based restoration techniques, fractional-order modeling, impedance spectroscopy and characterization, black-box-based approaches, and the current change method, often struggle to effectively determine model parameters. This difficulty arises from the inherent nonlinearity and multivariable complexity of PEMFC systems [19–22].

Consequently, metaheuristic optimization algorithms are gaining prominence as researchers seek to overcome the limitations of traditional methods. The advancement of computational power and artificial intelligence has spurred the development of numerous metaheuristic algorithms, which have proven highly effective in solving complex, nonlinear optimization problems. PEMFC parameter identification can be effectively framed as such an optimization problem [23]. Metaheuristic algorithms offer a compelling way to find optimal solutions with high accuracy and low computational cost. Consequently, many researchers have explored various metaheuristic algorithms to extract the unknown parameters that govern PEMFC behavior. These algorithms include established methods like differential evolution [24], biogeography-based optimization [25], JAYA and Nelder-Mead simplex [26], whale optimization [27], coyote optimization [28], bald eagle search optimizer [29], pathfinder algorithm [30], chaotic Harris Hawks optimization [31], artificial ecosystem optimizer [32], tree growth algorithm [33], marine predators and political optimizers [34], flower pollination algorithm [35], grasshopper optimizer [36], and atom search optimizer [37]. A summary of key observations from recent optimization strategies (2020–2024) is provided, noting that most methods use the sum of squared errors (SSE) as the primary objective function.

A literature review reveals that PEMFC parameter identification typically focuses on minimizing the sum of squared errors (SSE) between measured and estimated fuel cell voltage [38–45]. This work presents a novel approach by introducing the Huber loss function to this application for the first time. While existing methods focus on various optimization goals like accuracy, convergence speed, exploration–exploitation balance, and avoiding local minima, this study proposes a new metaheuristic algorithm [46–51]. This type of innovative approach has the potential to significantly advance the field and offer solutions to a range of engineering problems [52–56].

This summarizes recent research on PEMFC parameter identification, highlighting the employed optimization algorithms and their corresponding cost functions. A majority of these studies focus on minimizing the sum of squared errors (SSE) between measured and estimated fuel cell voltage. Several works have explored variations and hybridizations of existing metaheuristic algorithms. For instance, chaotic elements have been incorporated into algorithms like Harris Hawks optimization [31], particle swarm optimization [45], and Bonobo optimizer [53] to enhance exploration and avoid local minima. Hybrid approaches combining different algorithms, such as vortex search with differential evolution [39], gray wolf optimizer [40], Harris Hawks with atom search [44], and Osprey with coati optimization [55], have also been investigated. Furthermore, algorithms inspired by natural phenomena, including tree growth [33], moth–flame optimization [38], artificial ecosystem optimization [32, 41], coyote optimization [28], slime mould algorithm [42], and whale optimization [22], have been applied to this problem. Various other metaheuristic algorithms have been employed, such as the pathfinder algorithm [30], improved Archimedes optimization [43], heap-based optimization [47], bald eagle search [29, 50], gradient-based optimization [49], improved evaporation rate water cycle [51], improved gorilla troops [52], swarm intelligence algorithm [54], war strategy optimization [56], Kepler optimization [57], social learning–based optimization [58], spotted hyena optimizer [59], multistrategy tuna swarm optimization [60], dynamic ant colony optimization [61], enhanced slap swarm algorithm [62], improved walrus optimization [63], chaotic swarm intelligence [64], rime-ice algorithm [65], and exponential distribution optimizer [66]. While SSE is the most common cost function, some studies have explored alternatives like total standard deviation [33], relative error [43], mean absolute error (MAE) [22], power-based sum of absolute error [45], and mean squared error (MSE) [29, 48, 53].

The optimization algorithms and computational intelligence have undergone rapid development, and the efficiency and accuracy of solving complex engineering problems have increased tremendously. The efficiency of metaheuristic algorithms has been proven in recent studies in different areas such as photovoltaic parameter estimation [67], combined heat and power economic emission dispatch [68], and multiarea economic dispatch with renewable energy integration [69]. On the same note, better optimization methods like opposition-based learning and Laplacian crossover [70], enhanced hippopotamus optimization [71], and multiobjective brown bear optimization [72] have been observed to perform well in mechanical and structural design optimization. The comparative studies of metaheuristics also demonstrate their usefulness in constrained engineering problems [73], whereas hybrid methods (artificial neural networks and evolutionary algorithms) have been successful in designing

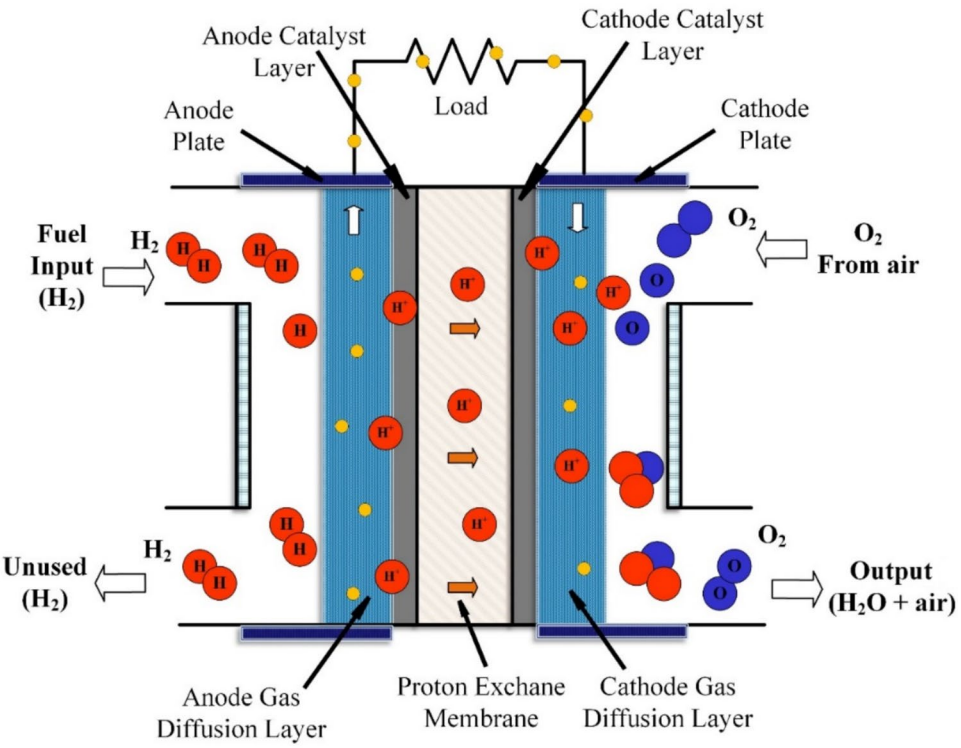

Fig. 1 Schematic diagram of PEMFC

structural components [74]. Also, more sophisticated predictive modeling methods, including TimesNet-GPR, have been used effectively to analyze fuel cell degradation under dynamic conditions [75]. Such advances highlight the increasing significance of intelligent optimization and machine learning in solving practical engineering problems.

The shortcomings of the current optimization algorithms like BBO and DE-BBO are well-established in the literature and are important in explaining the need for the proposed HG-BBO algorithm. The problem with traditional BBO is that it converges slowly and has a high probability of being trapped in local optima because of its use of fixed migration rates and a lack of exploration. Although DE-BBO is an improvement over BBO (adding differential evolution), it suffers the same issues of parameter tuning sensitivity and exploration–exploitation trade-off as BBO, especially in high-dimensional and nonlinear problems, such as estimating PEMFC parameters. The deficiencies result in suboptimal solutions and higher computational expenses. The proposed HG-BBO algorithm is able to overcome these shortcomings by a hybrid migration operator that linearly combines dynamic random heuristic crossover and exponentially dynamic random differential mutation, which improve local and global search abilities. Also, a global-best Gaussian mutation operator and random opposition learning are incorporated to further reduce premature convergence and enhance solution accuracy. The innovations allow HG-BBO to perform better than other methods in terms of convergence speed, robustness, and computational efficiency, as shown by the detailed comparative study of 12 PEMFC cases. The theoretical and practical importance of the algorithm in complex optimization problems is emphasized by its capacity to outperform the existing methods consistently.

The hybrid grouping biogeography-based optimization (HG-BBO) algorithm developed helps in solving the limitations that have been identified in the current optimization methods used in the parameter estimation of the proton exchange membrane fuel cell (PEMFC). Although there exist many algorithms, many of them have problems like slow convergence, the tendency to get stuck in local optima, and sensitivity to parameter tuning. These shortcomings make them ineffective in the accurate modeling of the highly nonlinear and multivariable nature of PEMFC systems. The HG-BBO algorithm presents a hybrid migration operator, which is a linearly dynamic random heuristic crossover and exponentially dynamic random differential mutation combination, and a global-best Gaussian mutation operator, to produce better exploration–exploitation balance. This combination of features allows more effective global search and still preserves the accuracy of local search, making the convergence faster and the quality of the solutions better than in the traditional approaches. Moreover, the simplicity of computation and the removal of unnecessary computations that the algorithm possesses fulfill the efficiency requirements of real-time optimization problems.

This work is the creation and use of the hybrid grouping biogeography-based optimization (HG-BBO) algorithm, which brings great innovations to the current optimization methods of PEMFC parameter estimation. The suggested algorithm incorporates a hybrid migration operator that is a combination of linearly dynamic random heuristic crossover and exponentially dynamic random differential mutation, which allows the balance of exploration and exploitation to be more effective. This method removes the calculation overhead of the emigration rate and increases the efficiency of the search by example-based learning. Also, the introduction of a global-best Gaussian mutation operator in the subsequent search stages enhances the convergence rate and accuracy of the solution. The algorithm also stands out by the random opposition learning, which does not cause premature convergence but does not add complexity to the computation. All these innovations share the common feature of overcoming some of the main drawbacks of the existing methods, namely, slow convergence, sensitivity to parameters, and local optima.

The hybrid grouping biogeography-based optimization (HG-BBO) algorithm shows clear superiority over other metaheuristic methods in the optimization of PEMFC parameters, especially in convergence speed, solution accuracy, and robustness. In contrast to the gray wolf optimizer (GWO) where exploration and exploitation are performed based on a hierarchical social structure, HG-BBO uses a hybrid migration operator along with global-best Gaussian mutation, which makes the transition between the global and local search smoother. Although GWO may be prone to premature convergence because of a strict leader–follower structure, the dynamic adaptation mechanisms of HG-BBO, including the linearly decreasing mutation rate, opposition-based learning, can help it escape local optima and preserve search efficiency.

Likewise, Harris Hawks optimization (HHO), a nature-inspired algorithm that simulates the collaborative hunting of hawks, has good exploratory power, but may not be able to refine solutions effectively in nonlinear optimization spaces that are very nonlinear. Conversely, the migration and mutation operators of HG-BBO that are biogeography-inspired offer a more systematic trade-off between exploration and exploitation and thus more stable convergence behavior. The search process is further refined by the incorporation of a sinusoidal model of migration to calculate the rate of immigration, which eliminates the likelihood of erratic convergence behavior, which is sometimes experienced in HHO.

As compared to evolutionary algorithms (EAs) that mainly rely on crossover and mutation operations, HG-BBO proves to be more adaptive to complex PEMFC models. Conventional EAs, like genetic algorithms (GAs), usually need a lot of parameter-tuning and may be computationally costly because they depend on random genetic operations. Conversely, the hybrid migration operator of HG-BBO, which is a hybrid between heuristic crossover and differential mutation, increases the diversity of solutions and reduces the amount of redundant computations. Also, the learning mechanism of the algorithm, which is based on opposition, adds another level of exploration, avoiding the stagnation in suboptimal areas, which is one of the weaknesses of standard EAs.

HG-BBO is better than current metaheuristics in parameter optimization of PEMFCs because it exploits the advantages of biogeography-based optimization and the power of hybridization techniques. It is well suited to the high-dimensional, nonlinear optimization problems of fuel cell modeling because it can sustain a strong balance between exploration and exploitation and because it has adaptive mutation and migration mechanisms. Its performance could also be confirmed in future through comparison with other hybrid metaheuristics, including hybrid GWO-PSO or adaptive HHO variations, to strengthen its position as a top optimization tool in energy systems.

The hybrid grouping biogeography-based optimization (HG-BBO) algorithm uses migration and mutation operators for local and global search, respectively. The hybrid grouping biogeography-based optimization (HG-BBO) algorithm is unique as compared to the existing methods because of a well-thought hierarchical structure that strategically combines the migration, mutation, and opposition-based learning operators in a phased manner. In contrast to the traditional hybrid algorithms, which merely mix several techniques, HG-BBO employs a three-level optimization structure with each of the elements being tailored and having different responsibilities depending on the search phase. The migration operator uses a linearly dynamic random heuristic crossover to perform localized refinement in the exploitation phases, whereas the mutation operator uses an exponentially dynamic random differential mechanism to explore globally. This hierarchical division of operations avoids the usual traps of operator interference that are found in other hybrid algorithms. Moreover, HG-BBO also incorporates a new global-best Gaussian mutation in later generations to speed up the convergence, as well as a selective opposition-based learning approach that only focuses on randomly chosen solutions in order to keep the computational efficiency. The theoretical benefits of the algorithm are its sinusoidal migration model and dynamic parameter adaptation mechanisms, which offer theoretical benefits in terms of balancing exploration–exploitation trade-offs, as the algorithm has shown to perform consistently across a variety of PEMFC configurations. This systematic hybridization strategy is proven to be more accurate (based on the low SSE values), converges faster (stability is reached after 40 iterations), and more robust (SDs are close to machine epsilon) than the current methods that use the same components in less coordinated

structures. The hierarchical combination of these operators in HG-BBO is a great improvement over the traditional hybrid implementations since it guarantees that each operator works best at the phase of the search that it is assigned to.

This hierarchical approach increases research efficiency and ensures a soft transition between exploration and exploitation. The key contributions of this research include the following:

- Optimization framework: developing HG-BBO as an arithmetic algorithm that efficiently balances exploration and exploitation for nonlinear PEMFC parameter optimization problems.
- Comprehensive benchmarking: evaluating HG-BBO against nine state-of-the-art algorithms, including PR-BBO, BBO-M, DE-BBO, Lx-BBO, BHCS, BLPSO, HBBOS, TD-BBO, and WR-BBO, to highlight its comparative strengths.
- PEMFC analysis: applying the HG-BBO framework to six distinct PEMFC stacks: BCS 500 W, Nedstack 600 W PS6, SR-12 W, Horizon H-12, Ballard Mark V, and STD 250 W to validate its versatility and robustness.
- Enhanced parameter estimation: achieving superior accuracy in minimizing the sum of squares error (SSE) between experimental and modeled data, with results consistently outperforming existing methods.
- Scalability and efficiency: demonstrating the scalability of HG-BBO across multiple PEMFC configurations, ensuring its adaptability to varying operational scenarios and design constraints.

The structure of this paper is as follows: "Modeling of PEMFC" discusses the mathematical modeling of PEMFCs and the challenges associated with parameter estimation. "Biogeography-based optimization with hybrid migration and global-best Gaussian mutation" introduces the HG-BBO framework and explains its operational phases. "Results and discussion" provides a comparative analysis with advanced algorithms, presents simulation results for 12 PEMFC configurations, and includes statistical analyses and sensitivity studies. Finally, "Conclusion" highlights the key findings and explores potential directions for future research.

Modeling of PEMFC

Figure 1 depicts the modeling of PEM fuel cells, which convert chemical energy into electrical energy. Hydrogen and oxygen are supplied to the anode and cathode, respectively. A thin membrane, the electrolyte, facilitates ion transport while blocking electron flow. Catalysts lower the activation energy needed for hydrogen oxidation. Ions migrate through the electrolyte, while electrons travel through an external circuit, producing an output voltage. A single PEMFC typically generates a voltage between 0.9 and 1.23 V. To satisfy higher power demands, multiple cells (N_{cells}) are connected in series, forming a PEMFC stack. The stack voltage (V_{stack}) is calculated using Eqs. (1) and (2) [2] [36].

$$V_{stack} = N_{cells} \times V_{cell} \tag{1}$$

$$\mathrm{V_{cell}} = E_{Nernst} - (V_{act} + V_{\Omega} + V_{com}) \tag{2}$$

The voltage of a single cell (V_{cell}) is composed of four elements: the Nernst open circuit voltage (E_{Nernst}) and three overpotential losses. E_{Nernst}, calculated under standard conditions using Eq. (3), represents the theoretical maximum voltage. The remaining three elements, representing losses, are activation losses (V_{act}), ohmic voltage drop (v_{Ω}), and concentration overpotential drop, also known as mass transport losses (v_{con}). These losses are calculated using Eqs. (8), (10), and (12), respectively [14].

$$E_{Nernest} = 1.229 - 85 \times 10^{-5}(\mathrm{T} - 298.15) + 4.3085 \times 10 - 5 * \mathrm{T}(\mathrm{I_n}(\mathrm{P_{H2}}\sqrt{\mathrm{P_{O2}}}) \tag{3}$$

$$\mathrm{P_{H2}} = \frac{\mathrm{RH_a} \times \mathrm{P_{H_2O}}}{2} \frac{1}{\left(\frac{\mathrm{RH_a P_{H_2O}}}{\mathrm{P_a}} \times \mathrm{e}^{\left(\frac{1.635\mathrm{I}}{\mathrm{A}}\right)(\mathrm{T}^{1.334})} - 1\right)} \tag{4}$$

$$\mathrm{P_{O_2}} = \left\{ \mathrm{RH_c} \times \mathrm{P_{H_2O}} \frac{1}{\left(\frac{\mathrm{RH_a P_{H_2O}}}{\mathrm{P_a}} \times \mathrm{e}^{\left(\frac{1.635\mathrm{I}}{\mathrm{A}}\right)(\mathrm{T}^{1.334})} - 1\right)} \right\} \text{For pure oxygen}$$

$$\mathrm{P_{O_2}} = \left\{ \mathrm{P_c} - \mathrm{RH_c} \times \mathrm{P_{H_2O}} - \frac{0.79}{0.21} \times \mathrm{P_{o2}} \times \mathrm{e}^{\left(\frac{0.291\mathrm{I}}{\mathrm{AT}0.832}\right)} \right\} \text{For naturalair} \tag{5}$$

$$\log_{10}\left(\mathrm{P_{H2O}}\right) = 2.95 \times \Delta\mathrm{T} \times 10^{-2} - 9.18 \times (\Delta\mathrm{T})^2 + 1.44 \times 10^{-7} \times (\Delta\mathrm{T})^3 - 2.18$$

$$\Delta\mathrm{T} = \mathrm{T} - 273.15 \tag{6}$$

The partial pressures of hydrogen (PH_2) and oxygen (PO_2), crucial for calculating the Nernst voltage, are determined using Eqs. (4) and (5), respectively. These equations consider factors like relative humidity at the cathode (RH_c) and anode (RH_a), saturation pressure of water vapor (PH_2O), and inlet pressures at the anode (P_a) and cathode (P_c). Equation (6) calculates PH_2O, with ΔT representing the difference between the cell temperature (T) and 273.15 (Eq. (7)). 'I' denotes the cell current, and 'A' represents the membrane's effective area. The cell's operational temperature (T) is typically below 100 °C.

$$V_{act} = -\left[\xi_1 + \xi_2 T + \xi_3 T \times I_n(C_{o2}) + \xi_4 T \times I_n(1)\right] \quad (7)$$

$$C_{o2} = \left(\frac{P_{o2}}{5.08 \times 10^6}\right) \times e^{\frac{498}{T}} \quad (8)$$

The voltage losses due to fuel cell loading are calculated using the following equations. Activation losses (V_{act}) are determined by Eq. (8), which incorporates semiempirical coefficients (ξ1 to ξ4) and the oxygen concentration (CO_2) at the catalytic layer Eq. (9). Ohmic voltage drop (V_Ω) across resistances is calculated using Eq. (10), where R_m is the membrane resistance and R_c is the contact resistance. The membrane's specific resistivity (ρ_m) is given by Eq. (11), which depends on factors like current density, temperature, and membrane water content (λ). Concentration drop in voltage (V_{con}) is calculated using Eq. (12), where β is a coefficient and J/J_{max} represents the ratio of current density to its maximum value.

$$V_\Omega = I(R_m \times R_c), R_m = \frac{\rho_{m \times l}}{A} \quad (9)$$

$$\rho_m = \frac{181.6\left[1 + 0.03\left(\frac{1}{A}\right) + 0.062\left(\frac{T}{303}\right)^2\left(\frac{1}{A}\right)^{2.5}\right]}{\left[\lambda - 0.634 - 3\left(\frac{1}{A}\right)\right] \times e^{[4.18(T-303/T]}} \quad (10)$$

$$V_{con} = -\beta l_n\left(1 - \frac{J}{J_{max}}\right) = -\beta, l_n(1 - \frac{\frac{1}{A}}{J_{max}}) \quad (11)$$

Accurately determining membrane water content (λ) can be difficult due to its fluctuating nature during operation. This study assumes a constant and acceptable water content across all operating conditions. Using a robust Huber loss function and the HGBBO algorithm, this study optimizes seven unknown parameters (λ, ξ1 to ξ4, R_c, and β). This optimization aims to develop an accurate PEMFC model suitable for simulation and research. Notably, some of these parameters are not typically available in manufacturer datasheets.

$$L_\delta = \left\{\begin{array}{c} 0.5(V_{sin} - V_{exp})^2 \text{if} \left|V_{sin} - V_{exp}\right| \le \delta \\ \delta\left(\left|V_{sin} - V_{exp}\right| - 0.5\delta\right) \text{otherwise} \end{array}\right\} \quad (12)$$

where L_δ is huber loss function.

A review of existing literature indicates that PEMFC parameter identification optimization primarily aims to minimize the sum of squared errors (SSE) between measured and estimated fuel cell voltages across a given dataset. This study introduces a novel approach. The current methods emphasize various optimization objectives, including accuracy, convergence speed, exploration–exploitation balance, and escaping local minima. The application of innovative metaheuristic algorithms, such as the one proposed here, has the potential to significantly advance the field and facilitate effective solutions to a range of engineering challenges. Numerous models have been employed to simulate the fuel cell *I-V* curve, each exhibiting varying performance.

Biogeography-based optimization with hybrid migration and global-best Gaussian mutation

The biogeography-based optimization (BBO) algorithm uses migration and mutation operators for local and global search, respectively [66]. To combat premature convergence and rotational variance, the two-stage differential BBO (TD-BBO) was developed [76]. TD-BBO incorporates the DE/current-to-rand/1 differential evolution strategy to improve local search and achieve rotational invariance. A two-stage mechanism enhances population diversity by using a sinusoidal migration model to calculate the immigration rate (λ) and a separate method for the emigration rate (μ). TD-BBO, while an improvement, still has limitations. While it uses a constant emigration rate (μ) in its first stage and a sinusoidal model in the second, along with Gaussian mutation and greedy selection, it suffers from an imbalance between exploration and exploitation. Its updating efficiency is low, as only solutions selected for immigration are updated. Furthermore, parameter tuning is complex, and the computational cost is high due to the calculation of immigration, emigration, and mutation rates, as well as the roulette wheel selection process. While the two-stage differential migration enhances exploitation, it can hinder convergence speed. Finally, although the Gaussian mutation provides some exploration, its effectiveness is limited and can also negatively impact convergence, especially in later search phases.

Hybrid migration operator

Linearly dynamic random heuristic crossover

TD-BBO's roulette wheel selection for emigration habitat selection is computationally expensive and inefficient [77]. Inspired by the natural process of homologous chromosome recombination, which creates new individuals, this work proposes a linearly dynamic random heuristic crossover to address these issues. This crossover method, detailed in Eq. (13), aims to improve search space exploration.

$$H_k(SIV_j) \leftarrow H_e(SIV_j) + w * (rand - 0.5) * (H_e(SIV_j) - H_k\left(SIV_j\right) \quad (13)$$

Table 1 Twelve PEMFC manufacturer sheets

S. no	Sheet 1	Sheet 2	Sheet 3	Sheet 4	Sheet 5	Sheet 6	Sheet 7	Sheet 8	Sheet 9	Sheet 10	Sheet 11	Sheet 12
PEMFC type	BCS 500 W	NetStack PS6	SR-12	H-12–1	Ballard Mark V	STD-1	Horizon	STD −2	STD −3	STD −4	H-12–2	H-12–3
Power (W)	500	6000	500	12	5000	250	500	250	250	250	12	13
N_{cells} (no.)	32	65	48	13	35	24	36	24	24	24	13	13
A (cm^2)	64	240	62.5	8.1	232	27	52	27	27	27	8.1	8.1
l (μm)	178	178	25	25	178	127	25	127	127	127	25	25
T (K)	333	343	323	323	343	343	338	343	343	343	302	312
J_{max} (mA/cm^2)	469	1125	672	246.9	1500	860	446	860	860	860	246.9	246.9
PH_2 (bar)	1.0	1.0	1.47628	0.4935	1.0	1.0	0.55	1.5	2.5	2.5	0.4	0.5
PO_2 (bar)	0.2095	1.0	0.2095	1.0	1.0	1.0	1.0	1.5	3.0	3.0	1.0	1.0

In this equation, w is a dynamically adjusted parameter, and (rand-0.5) generates a random number between − 0.5 and 0.5, representing the emigration habitat, selected using an example learning approach [78]. The immigration habitat, and SIV denotes the suitability index variables of a habitat. The example learning approach is crucial, as individuals learn and improve by emulating successful examples. This approach, used in the migration process, eliminates the need to calculate the emigration rate, thus reducing computational complexity. Habitats are ranked by fitness, and if the kth habitat is chosen for immigration, the emigration habitat is selected from the top $k-1$ habitats to ensure positive population evolution. The index of the chosen emigration habitat is randomly determined, as shown in the following equation Eq(14):

$$e = \text{ceil}((k - 1) * \text{rand}) \tag{14}$$

Here, ceil () rounds up to the nearest integer, and e is the index of the chosen emigration habitat. The dynamic parameter w decreases linearly from 1 to 0 as the current iteration number t increases, according to the following equation:

$$w = 1 - t/M \tag{15}$$

where M represents the maximum number of iterations. It is generally accepted that exploration should be emphasized in early search phases, while exploitation is more important later. Analyzing Eqs. (13) and (15), we see that early in the search, w and the difference between ($H_e(SIV_j)$ and $H_k(SIV_j)$)) $H_k(SIV_j) \leftarrow H_e(SIV_j)$ are larger. This leads to a wider search range around H_e, promoting population diversity and global search. Conversely, later in the search, both w and the difference between H $H_e(SIV_j)$ and $H_k(SIV_j)$ decrease [77], narrowing the search range around H_e and improving local search and convergence speed. Essentially, the current island H_k evolves towards better islands H_e making this crossover method more focused on exploitation. Finally, unlike TD-BBO, which calculates both immigration and emigration rates, this algorithm only calculates the immigration rate using the sinusoidal migration model, reducing the computational burden.

Exponentially dynamic random differential mutation

TD-BBO's migration process leaves some habitat features unchanged, potentially hindering search efficiency. To address this, an exponentially dynamic random differential mutation is introduced to update these nonmigrating features. This mutation approach is combined with the previously described linearly dynamic random heuristic crossover to create a hybrid migration operator. Differential evolution [79] is a powerful evolutionary algorithm that leverages the distance and direction between individuals to guide the

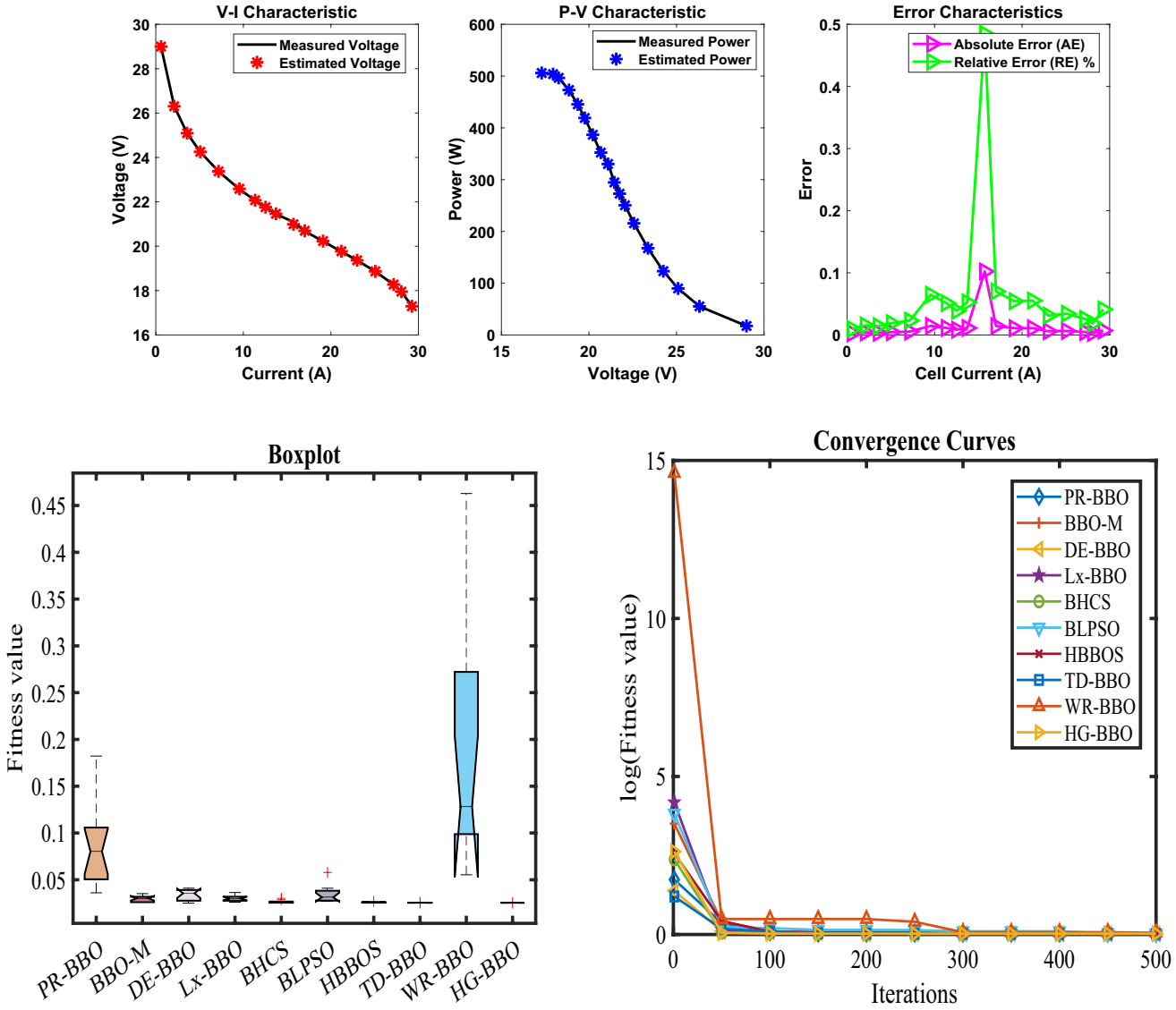

Fig. 2 Characteristic curves: **a** *P–V*, *V-I*, and error curve; **b** boxplot; and **c** convergence curve for sheet 1

search for better solutions. Inspired by this, a novel exponentially dynamic random mutation operator is proposed to enhance population diversity and global search. This operator uses two differential strategies, chosen with equal probability. If the linearly dynamic random heuristic crossover is not applied to certain features of a habitat, either Eq. (16) or (17) is randomly selected for execution with equal probability. These equations are defined as follows:

$$\begin{aligned} \mathrm{H_k}\left(\mathrm{SIV_j}\right) &= \mathrm{H_k}\left(\mathrm{SIV_j}\right) + \alpha * \mathrm{H_r}\left(\mathrm{SIV_j}\right) \\ &- \mathrm{H_n}\left(\mathrm{SIV_j}\right) + \mathrm{H_m}\left(\mathrm{SIV_j}\right) - \mathrm{H_h}\left(\mathrm{SIV_j}\right) \end{aligned} \tag{16}$$

$$\begin{aligned} \mathrm{H_k}\left(\mathrm{SIV_j}\right) &= \mathrm{H_k}\left(\mathrm{SIV_j}\right) + \alpha * \mathrm{H_{best}}\left(\mathrm{SIV_j}\right) \\ &- \mathrm{H_k}\left(\mathrm{SIV_j}\right) + \mathrm{H_r}\left(\mathrm{SIV_j}\right) - \mathrm{H_n}\left(\mathrm{SIV_j}\right) \end{aligned} \tag{17}$$

where $H_{\mathrm{best}}\left(\mathrm{SIV_j}\right)$ represents the best habitat in the current population, and$H_r\left(\mathrm{SIV}_j\right)$,$H_n\left(\mathrm{SIV}_j\right)$, $H_m\left(\mathrm{SIV}_j\right)$, and $H_h(\mathrm{SIV}_j)$ are randomly selected habitats, with $r, n, m, h, k \in [1, N]$ and $r \neq n \neq m \neq h \neq k$. α is an exponentially dynamic scale factor that controls the range of differential disturbance, defined by Eqs. (18) and (19):

$$\alpha = \mathrm{rand}^{\beta} \tag{18}$$

$$\beta = \beta_{\min} + (\beta_{\max} - \beta_{\min}) * \mathrm{t}/M \tag{19}$$

where $\beta_{\min}$ and $\beta_{\max}$ are minimum and maximum values of β, respectively.

Equation (18) shows that, unlike using a constant α, this method uses a random exponent with a wide fluctuation range (0 to 1), which can improve population diversity.

Table 2 Parameter optimization and function maximization for sheet 1

Algorithm	PR-BBO	BBO-M	DE-BBO	Lx-BBO	BHCS	BLPSO	HBBOS	TD-BBO	WR-BBO	HG-BBO
ξ_1	−1.19969	−0.95355	−0.8532	−1.19919	−0.93622	−0.95392	−1.00639	−1.01547	−1.05155	−0.90961
ξ_2	0.003962	0.002705	0.002374	0.003328	0.00279	0.003416	0.003443	0.00319	0.003178	0.002975
ξ_3	8.34E−05	5.04E−05	4.85E−05	4.3E−05	5.92E−05	9.6E−05	8.77E−05	6.97E−05	6.23E−05	7.63E−05
ξ_4	−0.0002	−0.00019	−0.00019	−0.00019	−0.00019	−0.00019	−0.00019	−0.00019	−0.00018	−0.00019
λ	23	22.99999	20.87729	21.98456	21.02195	22.301	21.18586	20.92116	16.10689	20.87724
R_C	0.000113	0.00033	0.0001	0.000185	0.000111	0.000134	0.0001	0.000102	0.000107	0.0001
B	0.01638	0.016022	0.016126	0.016244	0.016161	0.016789	0.016329	0.01614	0.013652	0.016126
Min	0.036077	0.025829	0.025493	0.025683	0.025506	0.026527	0.025604	0.025495	0.055335	0.025493
Max	0.182235	0.035187	0.041017	0.036426	0.030207	0.057813	0.026735	0.025588	0.462822	0.025493
Mean	0.087193	0.029308	0.034443	0.029941	0.026476	0.034346	0.025922	0.025517	0.189534	0.025493
Std	0.043845	0.003364	0.005981	0.00322	0.001429	0.008621	0.000304	3.01E−05	0.142293	3.37E−16
RT	9.09032	9.458132	7.863045	8.433612	17.29198	9.574993	9.152203	10.88156	17.53434	0.245247
FR	9.076923	5.615385	6.692308	5.692308	4.076923	6.923077	4	2.153846	9.769231	1

Table 3 Performance metrics of the proposed algorithm for sheet 1

Vcell	Icell	Vest	Pest	AE	Pref	MBE	RE %
29	0.6	28.99722	17.39833	0.002777	17.4	4.28E−07	0.009575
26.31	2.1	26.30594	55.24247	0.004063	55.251	9.17E−07	0.015443
25.09	3.58	25.09356	89.83493	0.003555	89.8222	7.02E−07	0.01417
24.25	5.08	24.25462	123.2135	0.00462	123.19	1.19E−06	0.019053
23.37	7.17	23.37542	167.6017	0.005416	167.5629	1.63E−06	0.023175
22.57	9.55	22.58461	215.6831	0.014615	215.5435	1.19E−05	0.064754
22.06	11.35	22.07133	250.5096	0.011327	250.381	7.13E−06	0.051348
21.75	12.54	21.75846	272.8511	0.008463	272.745	3.98E−06	0.038913
21.45	13.73	21.46126	294.6631	0.011263	294.5085	7.05E−06	0.052506
21.09	15.73	20.98774	330.1372	0.102258	331.7457	0.000581	0.484867
20.68	17.02	20.69451	352.2206	0.014509	351.9736	1.17E−05	0.070162
20.22	19.11	20.23099	386.6141	0.010986	386.4042	6.71E−06	0.054332
19.76	21.2	19.77094	419.144	0.010943	418.912	6.65E−06	0.055381
19.36	23	19.36602	445.4186	0.006025	445.28	2.02E−06	0.03112
18.86	25.08	18.86647	473.171	0.006466	473.0088	2.32E−06	0.034286
18.27	27.17	18.27472	496.5242	0.004721	496.3959	1.24E−06	0.025838
17.95	28.06	17.95331	503.7699	0.003311	503.677	6.09E−07	0.018444
17.3	29.26	17.29288	505.9896	0.007123	506.198	2.82E−06	0.041174
				0.012913		**3.61E−05**	**0.061363**

Equations (18) and (19) show that α is generated by a random exponent, and β, a dynamically adjusted parameter, varies from β_{min} to β_{max}, further enhancing the algorithm's flexibility. Equations demonstrate that a wider range for α leads to a broader search around$H_k$thus improving global search. Therefore, using the exponentially dynamic random factor is both necessary and effective. From Equations can see that early in the evolutionary process, β is small and α is large, resulting in a wide search range around H_k and facilitating exploration of potentially promising areas. Later on, β becomes large and α becomes small, narrowing the search range around H_k to enhance local search. Algorithm 1 presents the pseudocode for this hybrid migration operator, where N is the population size, D is the number of variables in the optimization problem, and rand generates a uniformly distributed random real number between 0 and 1.

Algorithm 1 The hybrid migration operator

Calculate the scaling factor α according to Eq. (18) and (19)for k = 1 to N dofor j = 1 to D do if rand < λk then Use the example learning approach to select He Update $H_k(SIV_j)$ by Eq. (13)else

if rand < 0.5 then Update$H_k SIV_j$ by Eq. (16)else

Update $H_k(SIV_j)$ by Eq. (17) end if end if end for end for

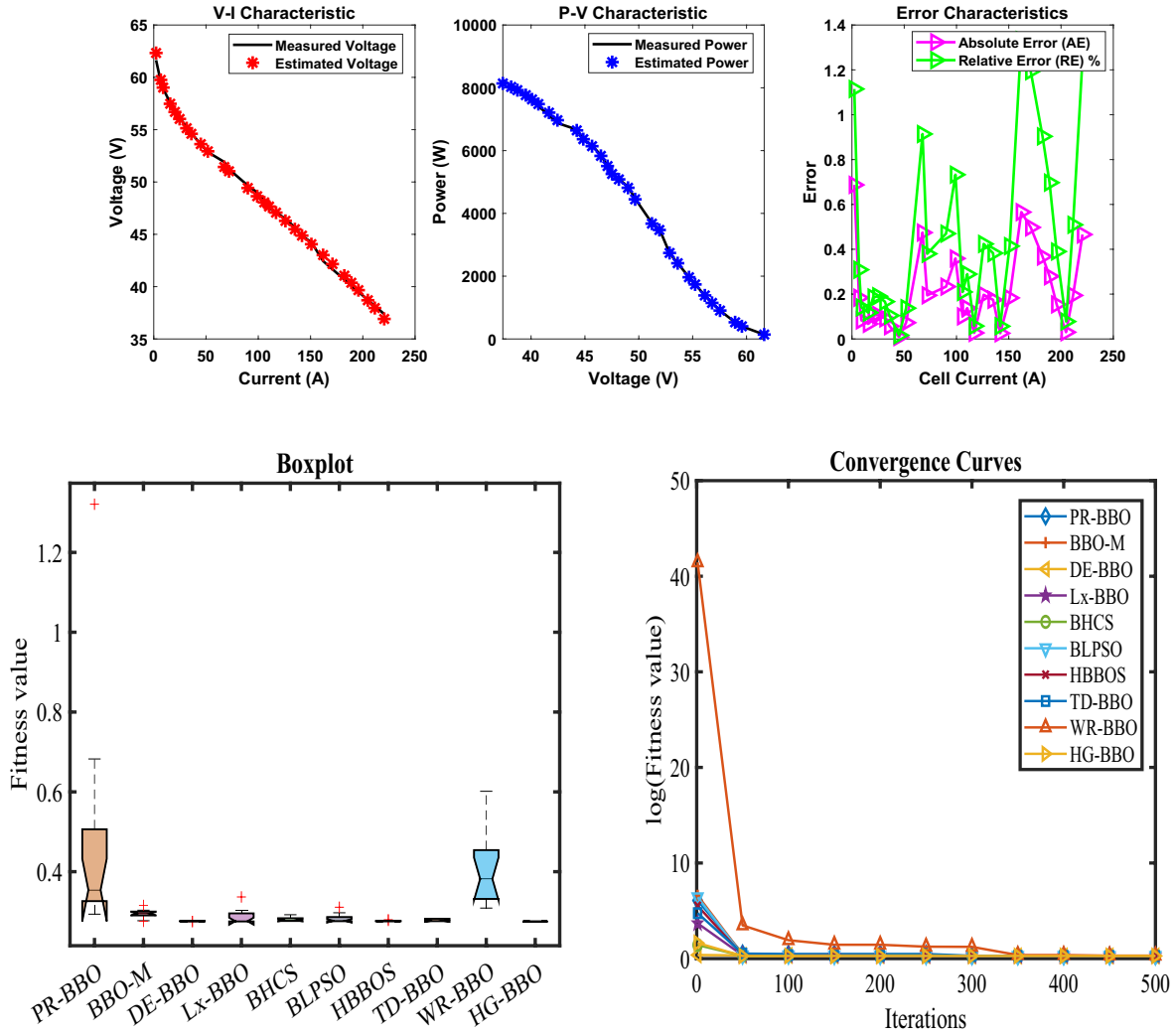

Fig. 3 Characteristic curves: **a** *P–V*, *V-I*, and error curve; **b** boxplot; and **c** convergence curve for sheet 2

Global-best Gaussian mutation operator

Previous work has explored using Gaussian, Cauchy, and Levy mutation operators within BBO [80], with Gaussian mutation also being used to improve exploration [81], including in TD-BBO. This paper simplifies the mutation process by removing the mutation rate calculation used in TD-BBO and instead employs a linearly decreasing mutation rate *mp*.This simplification reduces computational complexity. *mp* decreases with increasing iteration number, as shown in Eq. (20):

$$mp = mp_{\max} - (mp_{\max} - mp_{\min}) * t/M \tag{20}$$

This algorithm retains the Gaussian mutation operator from TD-BBO for the initial half of the search. As previously mentioned, exploration should be emphasized in the early stages, while exploitation becomes more critical later. Therefore, a global-best mutation operator is employed in the second half. Inspired by the global-best harmony search algorithm [82], this new global-best mutation operator is defined as follows:

$$\mathrm{cn} = \mathrm{ceil}(\mathrm{rand} * \mathrm{D}) \tag{21}$$

$$\mathrm{H_k(SIV_j)} \leftarrow \mathrm{SIV_{best}(SIV_{cn})} \tag{22}$$

Equation (20) shows that *mp* decreases linearly with increasing iteration number. Early in the search, *mp* larger, increasing the likelihood of Gaussian mutation. Later, when most habitats have good HSIs, *mp* is smaller, and the global-best mutation operator is used. This allows less fit habitats to learn from the global best, while preventing fitter habitats from regressing, thus improving convergence. Algorithm 2 provides the pseudocode for this global-best Gaussian mutation operator, where rand$n(0,1)$ generates Gaussian random numbers with a mean $\mu = 0$ and variance $\sigma^2 = 1$ [76].

Table 4 Parameter optimization and function maximization for sheet 2

Algorithm	PR-BBO	BBO-M	DE-BBO	Lx-BBO	BHCS	BLPSO	HBBOS	TD-BBO	WR-BBO	HG-BBO
ξ_1	−0.95109	−0.8532	−1.19969	−1.14704	−0.92221	−0.86042	−1.09547	−1.0689	−0.8532	−0.85418
ξ_2	0.003422	0.002398	0.003945	0.003609	0.002896	0.003088	0.003616	0.00316	0.003275	0.002429
ξ_3	8.9E−05	3.61E−05	7.43E−05	6.13E−05	5.71E−05	8.37E−05	7.24E−05	4.55E−05	0.000098	3.8E−05
ξ_4	−9.5E−05	−9.5E−05	−9.5E−05	−9.5E−05	−9.5E−05	−9.5E−05	−9.5E−05	−9.5E−05	−9.5E−05	−9.5E−05
λ	16.14864	14	14	14	14.00487	14	14.00782	14.03019	15.23396	14
R_C	0.000103	0.000105	0.00012	0.000117	0.000124	0.000117	0.000119	0.000118	0.000176	0.00012
B	0.038978	0.019031	0.016788	0.01731	0.016445	0.017263	0.017393	0.017581	0.025044	0.016788
Min	0.293527	0.275636	0.275211	0.275257	0.275293	0.275275	0.275617	0.275661	0.308782	0.275211
Max	1.320816	0.315484	0.276061	0.336715	0.292148	0.310939	0.279775	0.28344	0.601489	0.275211
Mean	0.468659	0.294237	0.275893	0.287861	0.280553	0.282769	0.276517	0.278848	0.404939	0.275211
Std	0.281767	0.010709	0.00031	0.017858	0.005288	0.011027	0.001134	0.003159	0.09208	2.61E−16
RT	12.65221	12.79053	11.24613	12.9428	23.00154	16.02975	12.35433	13.64153	23.55387	0.301204
FR	9.307692	7.230769	3.538462	4.769231	5.230769	5.230769	4.307692	4.923077	9.461538	1

Random opposition learning

To enhance global search capabilities, opposition-based learning [83] is incorporated. In this algorithm, a randomly selected habitat undergoes opposition-based learning, as shown in Eq. (23):

$$H_{ra} \leftarrow lb + (ub - H_{\text{best}}) \tag{23}$$

In this equation, H_{ra} represents a randomly chosen habitat from the current population, while *ub* and *lb* denote the upper and lower bounds of the habitat's values, respectively. Equation (23) essentially calculates the "opposite" of the randomly selected habitat and uses it as a new solution. This helps prevent the population from getting stuck in local optima. By applying opposition-based learning to only one randomly chosen habitat, the algorithm maintains efficiency without significantly increasing computational cost or requiring additional parameter tuning.

Algorithm 2 The global-best Gaussian mutation operator

Calculate the mutation rate
by Eq. (20) for k = 1 to N dofor j = 1 to D do if rand < m_p
then if t < M/2
$H_k(SIV_j)$=$H_k(SIV_j)$
randn (0,1) else Update H_k(SIVj)
by Eqs. (21) and (22) end ifend if end forend for

Other improvements

This algorithm, like TD-BBO, uses greedy selection instead of elitist selection to reduce runtime and eliminate a tuning parameter [84]. Furthermore, the immigration rate is calculated only once, outside the iteration loop, further reducing computational complexity (assuming fitness values remain valid). Algorithm 3 provides the algorithm's pseudocode. Key differences between this algorithm and TD-BBO. The key improvements of the proposed algorithm over TD-BBO are as follows: (1) this algorithm uses a hybrid migration operator instead of TD-BBO's two-stage differential migration. (2) TD-BBO calculates both immigration and emigration rates at each iteration using a two-stage mechanism. This algorithm eliminates emigration rate calculation and calculates the immigration rate (using the sinusoidal model) only once, outside the iteration loop. (3) TD-BBO uses Gaussian mutation, while this algorithm employs a novel global-best Gaussian mutation. TD-BBO calculates the mutation rate at each iteration, whereas this algorithm uses a linearly decreasing mutation rate. (4) This algorithm incorporates opposition-based learning to avoid local optima, a feature absent in TD-BBO. Similar to TD-BBO, this

Table 5 Performance metrics of the proposed algorithm for sheet 2

Vcell	Vest	Icell	Pest	AE	Pref	MBE	RE %
61.64	62.32708	2.25	140.2359	0.687083	138.69	0.016279	1.114671
59.57	59.75391	6.75	403.3389	0.183906	402.0975	0.001166	0.308722
58.94	59.02299	9	531.207	0.082995	530.46	0.000238	0.140813
57.54	57.47245	15.75	905.191	0.067553	906.255	0.000157	0.117401
56.8	56.69501	20.25	1148.074	0.104994	1150.2	0.00038	0.184848
56.13	56.02304	24.75	1386.57	0.106962	1389.218	0.000395	0.190562
55.23	55.13803	31.5	1736.848	0.091967	1739.745	0.000292	0.166516
54.66	54.60299	36	1965.708	0.057007	1967.76	0.000112	0.104294
53.61	53.61886	45	2412.849	0.008863	2412.45	2.71E−06	0.016533
52.86	52.93264	51.75	2739.264	0.072643	2735.505	0.000182	0.137426
51.91	51.43559	67.5	3471.902	0.474414	3503.925	0.007761	0.913916
51.22	51.02539	72	3673.828	0.194606	3687.84	0.001306	0.379942
49.66	49.42672	90	4448.405	0.233283	4469.4	0.001877	0.46976
49	48.64101	99	4815.46	0.358993	4851	0.004444	0.732639
48.15	48.04916	105.8	5083.601	0.100837	5094.27	0.000351	0.209422
47.52	47.6574	110.3	5256.611	0.137396	5241.456	0.000651	0.289134
47.1	47.07283	117	5507.521	0.02717	5510.7	2.55E−05	0.057687
46.48	46.28306	126	5831.665	0.196943	5856.48	0.001337	0.423715
45.66	45.4853	135	6140.516	0.174696	6164.1	0.001052	0.382603
44.85	44.87551	141.8	6363.347	0.025509	6359.73	2.24E−05	0.056876
44.24	44.05684	150.8	6643.772	0.183157	6671.392	0.001157	0.414008
42.45	43.01569	162	6968.542	0.565692	6876.9	0.011035	1.332607
41.66	42.15751	171	7208.934	0.49751	7123.86	0.008535	1.194214
40.68	41.04751	182.3	7482.96	0.367506	7415.964	0.004657	0.903408
40.09	40.36954	189	7629.843	0.279538	7577.01	0.002695	0.697275
39.51	39.66413	195.8	7766.236	0.154127	7736.058	0.000819	0.390097
38.73	38.69983	204.8	7925.726	0.030168	7931.904	3.14E−05	0.077892
38.15	37.95577	211.5	8027.646	0.194228	8068.725	0.001301	0.509117
37.38	36.91421	220.5	8139.583	0.465791	8242.29	0.007481	1.246096
				0.211225		**0.002612**	**0.453869**

algorithm uses greedy selection after migration and mutation to retain better habitats and improve solution accuracy and convergence. Finally, the population is sorted only once per generation to minimize computational overhead.

Algorithm 3 The procedure of our algorithm

Initialize the parameters and generate the population randomly Evaluate the HSI of each habitat and sort the population according to the HSI Calculate the immigration rate of each habitat for t = 1 to M do Perform Algorithm 1 Perform Algorithm 2 Select Hra randomly

Perform the opposition learning Limit the boundary of each new solution Calculate each habitat's HSI

Perform the greed selection Sort the population by their HSIs end for

This algorithm also distinguishes itself from other recent BBO variants like WR-BBO [85] and HBBOS [86]. While both WR-BBO and this algorithm improve computational efficiency, they do so differently. WR-BBO removes the mutation operator and compensates with a random-scaled differential mutation. This algorithm, however, uses a global-best Gaussian mutation and an exponentially dynamic random differential mutation to enhance global search. WR-BBO employs a dynamic heuristic crossover for local search, while this algorithm uses a linearly dynamic random heuristic crossover. Both use opposition-based learning, but WR-BBO applies it to the worst habitat, while this algorithm applies it to a random one. Similarities include replacing roulette wheel selection with example learning, using greedy selection, and calculating the immigration rate outside the iteration loop.

Results and discussion

Researcher's optimized settings for 12 different PEMFC stacks (BCS 500 W [87] [88], Nedstack 600 W PS6 [87] [88], SR-12 W [87] [88], Horizon H-12 [89], Ballard Mark V [90], and STD 250 W [90]) using both experiments and

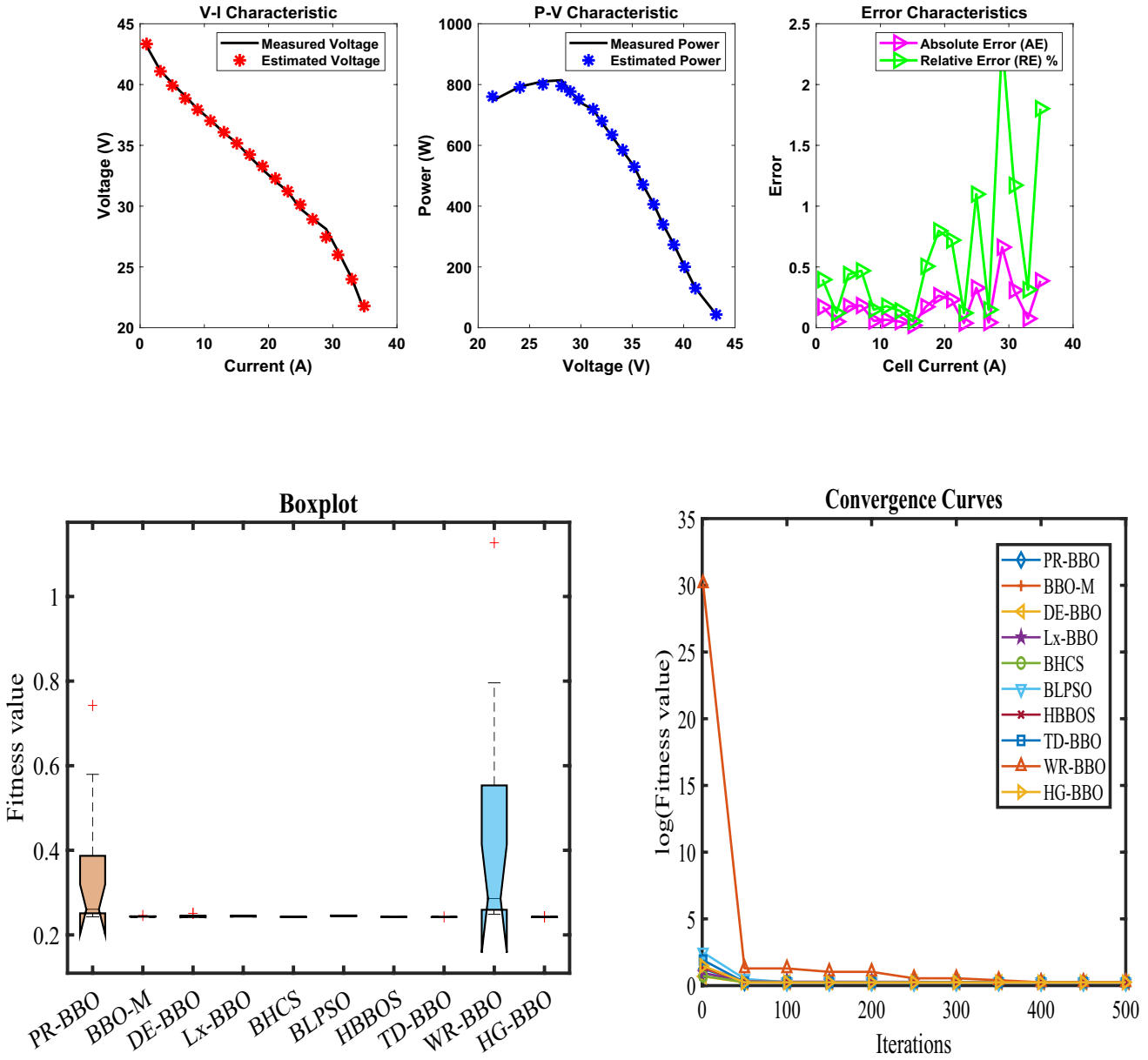

Fig. 4 Characteristic curves: **a** P–V, V-I, and error curve; **b** boxplot; and **c** convergence curve for sheet 3

computer modeling. For the experiments, they used voltage-current data from manufacturers and also took real-time measurements of gas pressure and cell temperature using digital multimeters, pressure sensors, and thermocouples.

The 12 PEMFC stacks selected for evaluation were chosen to ensure a comprehensive assessment of the proposed algorithm's performance across varying power ranges, operating conditions, and real-world applications. The stacks span a broad spectrum of power outputs—from small-scale systems like the 12 W Horizon H-12 (suitable for portable electronics) to high-power industrial units such as the 6 kW Nedstack PS6—ensuring that the algorithm is tested under diverse load demands. Additionally, the tested stacks cover different configurations, including low-temperature (302–343 K) and high-pressure (up to 3.0 bar) conditions, as well as varying membrane properties (thickness: 25–178 µm, active area: 8.1–240 cm^2).

To enhance credibility and reproducibility, the study prioritizes publicly available datasets from well-documented PEMFC manufacturers, including BCS, Ballard, and Horizon, which are widely referenced in fuel cell research. For instance, the BCS 500 W and Ballard Mark V datasets have been extensively used in prior PEMFC modeling studies, allowing for direct comparison with existing optimization methods. Furthermore, the inclusion of both pure oxygen

Table 6 Parameter optimization and function maximization for sheet 3

Algorithm	PR-BBO	BBO-M	DE-BBO	Lx-BBO	BHCS	BLPSO	HBBOS	TD-BBO	WR-BBO	HG-BBO
ξ_1	−0.92259	−0.8532	−1.19969	−0.94099	−0.9949	−1.19969	−0.96618	−1.02189	−0.88878	−0.8532
ξ_2	0.003461	0.00286	0.003361	0.003154	0.002806	0.003398	0.002901	0.003598	0.003294	0.002536
ξ_3	0.000098	7.29E−05	0.000036	7.44E−05	4.11E−05	3.84E−05	5.3E−05	8.68E−05	9.44E−05	5.2E−05
ξ_4	−9.5E−05	−9.5E−05	−9.5E−05	−9.5E−05	−9.5E−05	−9.5E−05	−9.5E−05	−9.5E−05	−9.5E−05	−9.5E−05
λ	20.84768	23	23	17.21202	22.86185	19.06355	22.18392	22.98428	21.2269	23
R_C	0.000537	0.000665	0.000673	0.000592	0.000648	0.000632	0.000647	0.000679	0.000385	0.000673
B	0.177284	0.17548	0.17532	0.174657	0.175833	0.175106	0.175617	0.175176	0.178593	0.17532
Min	0.242736	0.242286	0.242284	0.242582	0.242339	0.242605	0.242319	0.242289	0.248645	0.242284
Max	0.742508	0.245998	0.250872	0.246044	0.242971	0.246301	0.242544	0.242429	1.126999	0.242927
Mean	0.351164	0.243636	0.244301	0.244257	0.242546	0.244779	0.242429	0.242323	0.442078	0.242433
Std	0.153524	0.001062	0.003168	0.001141	0.000177	0.001204	6.64E−05	4.01E−05	0.275597	0.000282
RT	8.515136	8.821301	7.682852	8.269485	16.81479	8.927765	9.142363	10.29496	17.01984	0.220322
FR	8.923077	5.846154	4.538462	7	3.846154	7.307692	3.538462	2.384615	9.615385	2

(Nedstack PS6) and natural air-fed (SR-12, STD 250 W) cathode configurations ensures that the algorithm is validated under different reactant supply conditions.

While the current study demonstrates the algorithm's effectiveness across these representative cases, future work could expand validation using additional open-access datasets, such as those from the IEEE PES Fuel Cell Database or experimental data published in peer-reviewed repositories. This would further reinforce the generalizability of the proposed method and provide a more extensive benchmark for comparison with alternative optimization techniques.

By systematically evaluating the algorithm across different power levels, operating pressures, temperatures, and membrane properties, this study ensures that the results are not only statistically robust but also applicable to a wide range of PEMFC systems in real-world scenarios. The strong alignment between simulation and experimental data across all 12 cases further validates the algorithm's reliability and adaptability.

Detailed specifications for each PEMFC model are available in Table 1. For the computer modeling part, they used the hybrid grouping biogeography-based optimization (HG-BBO) to estimate the best parameters. The HG-BBO algorithm is designed with a phased approach (like elementary, middle, and high school levels) to effectively search for the best solutions. This optimization aimed to minimize the sum of squared errors (SSE) between the experimentally measured voltage values and those predicted by the model. The performance of the HG-BBO algorithm was evaluated against nine advanced optimization algorithms (PR-BBO, BBO-M, DE-BBO, Lx-BBO, BHCS, BLPSO, HBBOS, TD-BBO, and WR-BBO). All simulations were conducted in MATLAB R2023a with a group size of 40 and a maximum of 500 iterations.

HG-BBO algorithm uses a mixture of both boundary constraint treatment and feasibility maintenance methods to treat constraints efficiently throughout the optimization process. The boundary constraints are handled by a reflection mechanism, in which any solution that is outside the parameter bounds is reflected back into the search space of feasible solutions. This method preserves the diversity of the population and still keeps all the solutions within physically feasible limits of PEMFC parameters. In more complicated constraints where there are interdependencies between the parameters, the algorithm will use a penalty function approach where it will dynamically modify the fitness value of infeasible solutions depending on the extent of the constraint violation. The constraint handling strategy is hierarchical in nature, i.e., boundary violations are corrected first, followed by the feasibility-based selection in the course of migration operations. This twofold strategy guarantees the evolutionary process involves only solutions that are feasible or slightly violating and does not compromise

Table 7 Performance metrics of the proposed algorithm for sheet 3

Vcell	Vest	Icell	Pest	AE	Pref	MBE	RE %
43.17	43.34081	1.004	43.51417	0.170809	43.34268	0.001621	0.395667
41.14	41.09008	3.166	130.0912	0.049922	130.2492	0.000138	0.121347
40.09	39.91451	5.019	200.3309	0.175488	201.2117	0.001711	0.437735
39.04	38.85715	7.027	273.0492	0.182848	274.3341	0.001857	0.46836
37.99	37.93346	8.958	339.808	0.056535	340.3144	0.000178	0.148816
37.08	37.01454	10.97	406.0495	0.065463	406.7676	0.000238	0.176546
36.03	36.07991	13.05	470.8428	0.049906	470.1915	0.000138	0.138511
35.19	35.17136	15.06	529.6807	0.018636	529.9614	1.93E − 05	0.052958
34.07	34.24209	17.07	584.5124	0.172088	581.5749	0.001645	0.505102
33.02	33.28313	19.07	634.7092	0.263126	629.6914	0.003846	0.796869
32.04	32.2707	21.08	680.2664	0.2307	675.4032	0.002957	0.720038
31.2	31.23769	23.01	718.7793	0.037694	717.912	7.89E − 05	0.120813
29.8	30.12737	24.94	751.3766	0.327372	743.212	0.005954	1.098562
28.96	28.91713	26.87	777.0034	0.042866	778.1552	0.000102	0.148018
28.12	27.45776	28.96	795.1766	0.662243	814.3552	0.024365	2.355061
26.3	25.9918	30.81	800.8075	0.308195	810.303	0.005277	1.171846
24.06	23.98487	32.97	790.7811	0.075131	793.2582	0.000314	0.312265
21.4	21.78563	34.9	760.3186	0.385634	746.86	0.008262	1.802027
				0.181925		**0.003261**	**0.609475**

the exploratory power of the algorithm. The mutation operators use Gaussian sampling with mean correction to bias exploration toward more feasible regions, especially useful when some parameters have strict physical constraints such as water content of the membrane and ohmic resistance. Also, the global-best mutation stage employs the elite solutions which by definition meet all the constraints and further directs the population toward the feasible optima. These constraint handling mechanisms are synergistic with the hybrid migration operators used in HG-BBO since the optimization performance and constraint satisfaction must be balanced, which is of utmost importance in accurate estimation of PEMFC parameters where physical realizability is a primary concern. The high performance of the algorithm in handling constraints is demonstrated by the fact that it produced feasible solutions in all 12 PEMFC test cases and still performed better in optimization.

Sheet 1

Analysis of PEMFC system sheet 1 revealed that the HG-BBO algorithm significantly outperformed nine other optimization algorithms. HG-BBO achieved the highest accuracy in estimating key parameters ($\xi_1 = -0.90961$, $\xi_2 = 0.002975$, $\xi_3 = 7.63\text{E} - 05$), the lowest average error (0.025493) with minimal standard deviation ($3.37\text{E} - 16$), and the fastest processing time (0.245247 s). Its Friedman ranking of 1 indicated superior speed and reliability. Figure 2a demonstrated HG-BBO's accuracy in replicating *V-I* and *P–V* curves, while Fig. 2b showed its stability compared to WR-BBO, TD-BBO, and HBBOS. Figure 2c showed HG-BBO's rapid convergence. These results, supported by detailed data in Tables 2 and 3, confirm HG-BBO's exceptional performance in PEMFC parameter optimization due to its effective three-phase design.

Sheet 2

Analysis of PEMFC system sheet 2 revealed that the HG-BBO algorithm significantly outperformed nine other optimization algorithms. HG-BBO achieved the highest accuracy in estimating key parameters ($\xi_1 = -0.85418$, $\xi_2 = 0.002429$, $\xi_3 = 3.8\text{E} - 05$), the lowest average error (0.275211) with minimal standard deviation ($2.61\text{E} - 16$), and the fastest processing time (0.301204 s). Its Friedman ranking of 1 indicated superior speed and reliability. Figure 3a demonstrated HG-BBO's accuracy in replicating *V-I* and *P–V* curves, while Fig. 3b showed its stability compared to WR-BBO, TD-BBO, and HBBOS. Figure 3c showed HG-BBO's rapid convergence. These results, supported by detailed data in Tables 4 and 5, confirm HG-BBO's exceptional performance in PEMFC parameter optimization due to its effective three-phase design.

Sheet 3

Analysis of PEMFC system sheet 3 revealed that the HG-BBO algorithm significantly outperformed nine other optimization algorithms. HG-BBO achieved the highest accuracy in estimating key parameters ($\xi_1 = -0.8532$,

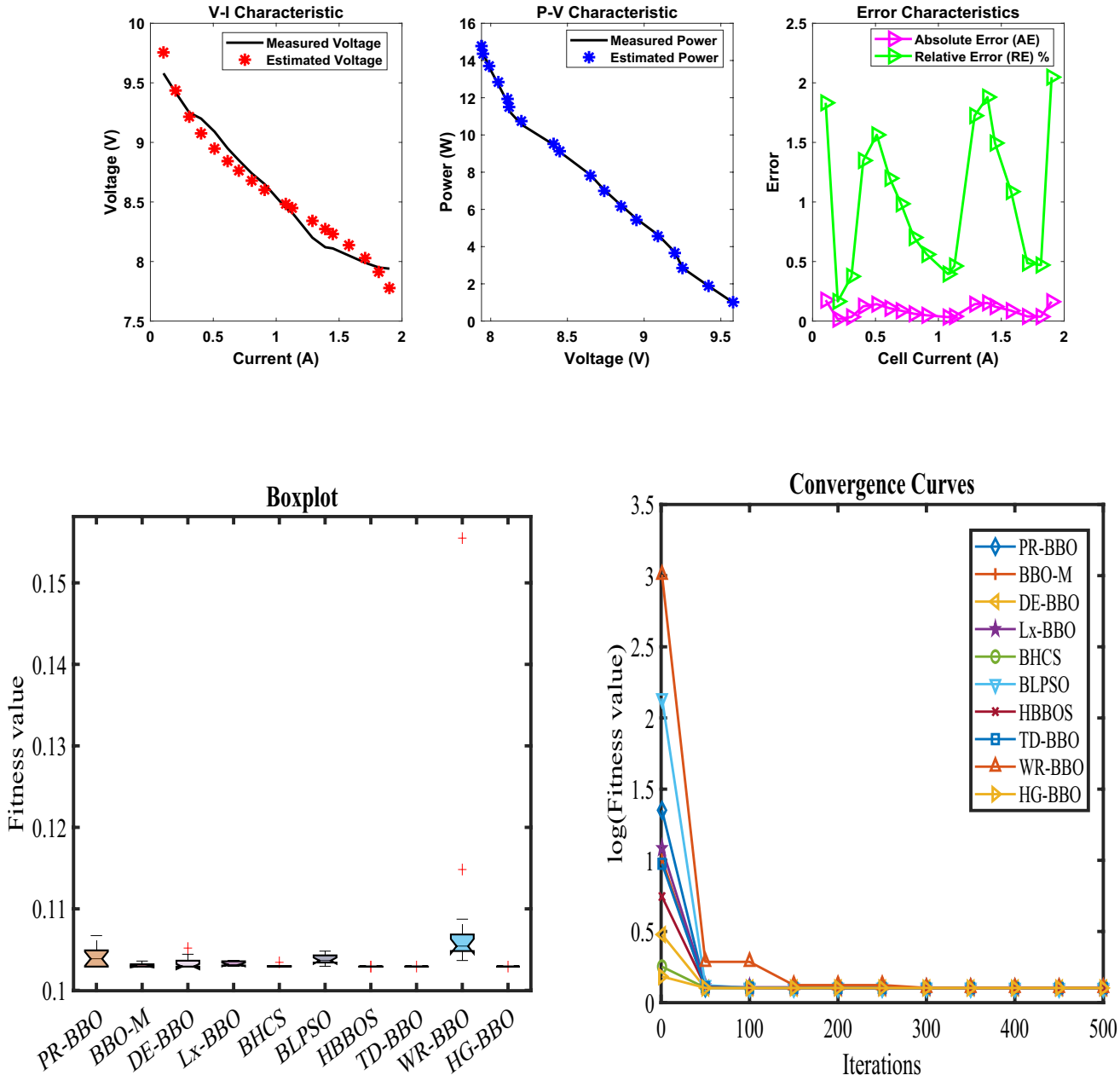

Fig. 5 Characteristic curves: **a** P–V, V-I, and error curve; **b** box plot; and **c** convergence curve for sheet 4

$\xi_2 = 0.002536$, $\xi_3 = 5.2\text{E}-05$), the lowest average error (0.242433) with minimal standard deviation (0.000282), and the fastest processing time (0.220322 s). Its Friedman ranking of 2 indicated superior speed and reliability. Figure 4a demonstrated HG-BBO's accuracy in replicating *V-I* and *P–V* curves, while Fig. 4b showed its stability compared to WR-BBO, TD-BBO, and HBBOS. Figure 4c showed HG-BBO's rapid convergence. These results, supported by detailed data in Tables 6 and 7, confirm HG-BBO's exceptional performance in PEMFC parameter optimization due to its effective three-phase design.

Sheet 4

Analysis of PEMFC system sheet 4 revealed that the HG-BBO algorithm significantly outperformed nine other optimization algorithms. HG-BBO achieved the highest accuracy in estimating key parameters ($\xi_1 = -1.19969$, $\xi_2 = 0.002817$, $\xi_3 = 5.29\text{E}-05$), the lowest average error (0.102915) with minimal standard deviation (7.9E−17), and the fastest processing time (0.205601 s). Its Friedman ranking of 1.230769 indicated superior speed and reliability. Figure 5a demonstrated HG-BBO's accuracy in replicating *V-I*

Table 8 Parameter optimization and function maximization for sheet 4

Algorithm	PR-BBO	BBO-M	DE-BBO	Lx-BBO	BHCS	BLPSO	HBBOS	TD-BBO	WR-BBO	HG-BBO
ξ_1	−0.94141	−0.8532	−1.19969	−0.97006	−1.19826	−0.86013	−0.88126	−1.10778	−1.13568	−1.19969
ξ_2	0.002127	0.001509	0.003445	0.002587	0.002938	0.002042	0.002448	0.002423	0.002507	0.002817
ξ_3	6.08E−05	0.000036	0.000098	8.75E−05	6.19E−05	7.28E−05	9.72E−05	4.51E−05	4.5E−05	5.29E−05
ξ_4	−0.00011	−0.00011	−0.00011	−0.00011	−0.00011	−0.00011	−0.00011	−0.00011	−0.00011	−0.00011
λ	14	14	14	14.02102	14	14	14	14.00146	14.62364	14
R_C	0.0008	0.0008	0.0008	0.000797	0.0008	0.000762	0.0008	0.0008	0.000378	0.0008
B	0.0136	0.0136	0.0136	0.0136	0.013601	0.0136	0.0136	0.0136	0.013944	0.0136
Min	0.102915	0.102915	0.102915	0.102926	0.102915	0.102957	0.102915	0.102916	0.103663	0.102915
Max	0.106718	0.103596	0.105186	0.103652	0.10344	0.104817	0.102918	0.102922	0.155491	0.102915
Mean	0.104078	0.103079	0.103429	0.103262	0.102985	0.103818	0.102916	0.102917	0.110036	0.102915
Std	0.001277	0.000214	0.000714	0.000276	0.000139	0.000629	1.09E−06	1.63E−06	0.013956	7.9E−17
RT	8.799977	9.005837	7.685694	8.379502	16.79896	9.040695	9.072234	10.521	17.14831	0.205601
FR	7	4.769231	4.615385	7	5.230769	7.769231	3.384615	4.307692	9.692308	1.230769

Table 9 Performance metrics of the proposed algorithm for Sheet 4

Vcell	Vest	Icell	Pest	AE	Pref	MBE	RE %
9.58	9.755532	0.104	1.014575	0.175532	0.99632	0.001712	1.832272
9.42	9.435534	0.2	1.887107	0.015534	1.884	1.34E−05	0.164909
9.25	9.215306	0.309	2.84753	0.034694	2.85825	6.69E−05	0.37507
9.2	9.075995	0.403	3.657626	0.124005	3.7076	0.000854	1.347879
9.09	8.947893	0.51	4.563425	0.142107	4.6359	0.001122	1.563338
8.95	8.842715	0.614	5.429427	0.107285	5.4953	0.000639	1.19872
8.85	8.762861	0.703	6.160291	0.087139	6.22155	0.000422	0.984618
8.74	8.678685	0.806	6.99502	0.061315	7.04444	0.000209	0.70154
8.65	8.601587	0.908	7.810241	0.048413	7.8542	0.00013	0.559683
8.45	8.483394	1.076	9.128131	0.033394	9.0922	6.2E−05	0.39519
8.41	8.448867	1.127	9.521873	0.038867	9.47807	8.39E−05	0.462156
8.2	8.341384	1.288	10.7437	0.141384	10.5616	0.001111	1.724194
8.12	8.272663	1.39	11.499	0.152663	11.2868	0.001295	1.880081
8.11	8.231198	1.45	11.93524	0.121198	11.7595	0.000816	1.494432
8.05	8.137515	1.578	12.841	0.087515	12.7029	0.000425	1.087138
7.99	8.028856	1.707	13.70526	0.038856	13.63893	8.39E−05	0.486306
7.95	7.912602	1.815	14.36137	0.037398	14.42925	7.77E−05	0.47041
7.94	7.777413	1.9	14.77708	0.162587	15.086	0.001469	2.047696
				0.089438		**0.000588**	**1.043091**

and *P–V* curves, while Fig. 5b showed its stability compared to WR-BBO, TD-BBO, and HBBOS. Figure 5c showed HG-BBO's rapid convergence. These results, supported by detailed data in Tables 8 and 9, confirm HG-BBO's exceptional performance in PEMFC parameter optimization due to its effective three-phase design.

Sheet 5

Analysis of PEMFC system sheet 5 revealed that the HG-BBO algorithm significantly outperformed nine other optimization algorithms. HG-BBO achieved the highest accuracy in estimating key parameters ($\xi_1 = -0.90284$, $\xi_2 = 0.002857$, $\xi_3 = 6.84\text{E}-05$), the lowest average error (0.148632) with minimal standard deviation (4.62E−08), and the fastest processing time (0.218836 s). Its Friedman ranking of 1 indicated superior speed and reliability. Figure 6a demonstrated HG-BBO's accuracy in replicating *V-I* and *P–V* curves, while Fig. 6b showed its stability compared to WR-BBO, TD-BBO, and HBBOS. Figure 6c showed HG-BBO's rapid convergence. These results, supported by detailed data in Tables 10 and 11, confirm HG-BBO's exceptional performance in PEMFC parameter optimization due to its effective three-phase design.

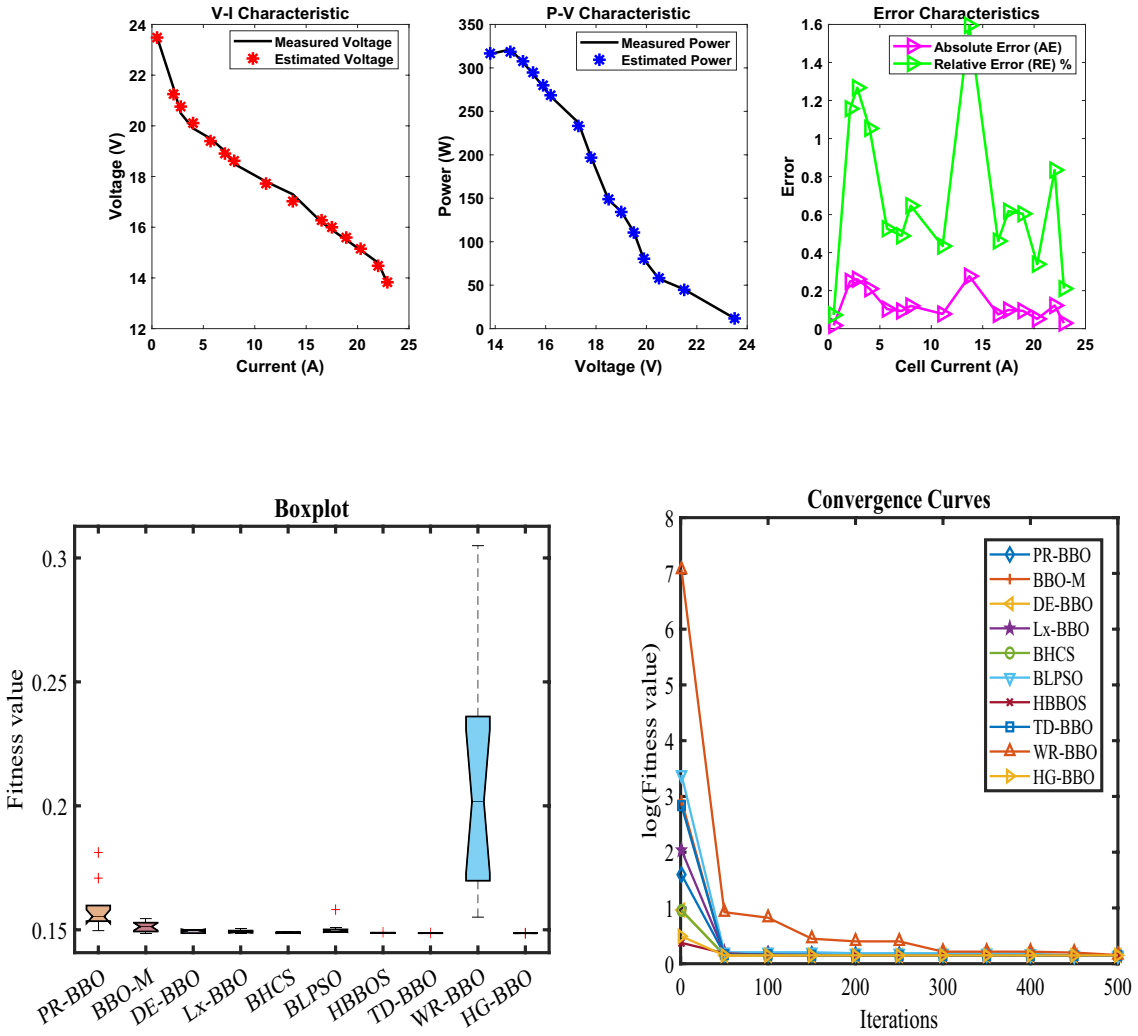

Fig. 6 Characteristic curves: **a** *P–V*, *V-I*, and error curve; **b** box plot; and **c** convergence curve for sheet 5

Table 10 Parameter optimization and function maximization for sheet 5

Algorithm	PR-BBO	BBO-M	DE-BBO	Lx-BBO	BHCS	BLPSO	HBBOS	TD-BBO	WR-BBO	HG-BBO
ξ_1	−0.94631	−0.92825	−0.96321	−1.03638	−1.09989	−0.93193	−0.91067	−0.99988	−1.14277	−0.90284
ξ_2	0.002546	0.00279	0.002587	0.002972	0.003164	0.002745	0.002793	0.002961	0.003428	0.002857
ξ_3	3.73E−05	5.83E−05	3.66E−05	4.88E−05	4.93E−05	5.43E−05	6.22E−05	5.56E−05	5.9E−05	6.84E−05
ξ_4	−0.00017	−0.00017	−0.00017	−0.00017	−0.00017	−0.00017	−0.00017	−0.00017	−0.00018	−0.00017
λ	15.06998	14.31503	14.43913	14.57856	14.38601	14.7561	14.40723	14.44553	16.1672	14.43913
R_C	0.000533	0.0001	0.0001	0.000107	0.000101	0.000231	0.0001	0.0001	0.000397	0.0001
B	0.01367	0.0136	0.013795	0.013873	0.013755	0.013977	0.013734	0.013802	0.013657	0.013795
Min	0.149657	0.148652	0.148632	0.148696	0.148645	0.148869	0.148645	0.148633	0.155094	0.148632
Max	0.181182	0.154507	0.149959	0.150448	0.149322	0.158144	0.148997	0.148722	0.304957	0.148632
Mean	0.158448	0.151202	0.149341	0.149341	0.14885	0.150228	0.148775	0.148648	0.207977	0.148632
Std	0.008715	0.002143	0.000593	0.000551	0.000244	0.00245	8.75E−05	2.36E−05	0.049051	4.62E−08
RT	7.725349	7.989175	6.947368	7.556727	14.67608	8.129268	8.054184	9.620897	15.50531	0.218836
FR	8.769231	7	4.923077	6	4	6.769231	4.076923	2.615385	9.846154	1

Table 11 Performance metrics of the proposed algorithm for sheet 5

Vcell	Vest	Icell	Pest	AE	Pref	MBE	RE %
23.5	23.48309	0.5	11.74154	0.016914	11.75	1.91E − 05	0.071975
21.5	21.2513	2.1	44.62774	0.248696	45.15	0.004123	1.156727
20.5	20.75981	2.8	58.12748	0.259815	57.4	0.0045	1.267389
19.9	20.10958	4	80.43831	0.209577	79.6	0.002928	1.053152
19.5	19.39753	5.7	110.5659	0.102468	111.15	0.0007	0.525477
19	18.90725	7.1	134.2415	0.092746	134.9	0.000573	0.488139
18.5	18.61964	8	148.9571	0.11964	148	0.000954	0.646705
17.8	17.72275	11.1	196.7226	0.077246	197.58	0.000398	0.433969
17.3	17.02409	13.7	233.23	0.275911	237.01	0.005075	1.594863
16.2	16.27464	16.5	268.5316	0.074644	267.3	0.000371	0.460763
15.9	15.99828	17.5	279.9699	0.09828	278.25	0.000644	0.618116
15.5	15.59366	18.9	294.7201	0.093658	292.95	0.000585	0.604245
15.1	15.15114	20.3	307.5681	0.05114	306.53	0.000174	0.338674
14.6	14.47819	22	318.5201	0.121813	321.2	0.000989	0.834336
13.8	13.82904	22.9	316.685	0.029041	316.02	5.62E − 05	0.210444
				0.124773		**0.001473**	**0.686998**

Sheet 6

Analysis of PEMFC system sheet 6 revealed that the HG-BBO algorithm significantly outperformed nine other optimization algorithms. HG-BBO achieved the highest accuracy in estimating key parameters ($\xi_1 = -1.19939$, $\xi_2 = 0.003769$, $\xi_3 = 0.000098$), the lowest average error (0.283774) with minimal standard deviation (2.97E − 16), and the fastest processing time (0.195683 s). Its Friedman ranking of 1 indicated superior speed and reliability. Figure 7a demonstrated HG-BBO's accuracy in replicating *V-I* and *P–V* curves, while Fig. 7b showed its stability compared to WR-BBO, TD-BBO, and HBBOS. Figure 7c showed HG-BBO's rapid convergence. These results, supported by detailed data in Tables 12 and 13, confirm HG-BBO's exceptional performance in PEMFC parameter optimization due to its effective three-phase design.

Sheet 7

Analysis of PEMFC system sheet 7 revealed that the HG-BBO algorithm significantly outperformed nine other optimization algorithms. HG-BBO achieved the highest accuracy in estimating key parameters ($\xi_1 = -1.19526$, $\xi_2 = 0.003291$, $\xi_3 = 5.67\text{E} - 05$), the lowest average error (0.121755) with minimal standard deviation (4.97E − 16), and the fastest processing time (0.187506 s). Its Friedman ranking of 1.076923 indicated superior speed and reliability. Figure 8a demonstrated HG-BBO's accuracy in replicating *V-I* and *P–V* curves, while Fig. 8b showed its stability compared to WR-BBO, TD-BBO, and HBBOS. Figure 8c showed HG-BBO's rapid convergence. These results, supported by detailed data in Tables 14 and 15, confirm HG-BBO's exceptional performance in PEMFC parameter optimization due to its effective three-phase design.

Sheet 8

Analysis of PEMFC system sheet 8 revealed that the HG-BBO algorithm significantly outperformed nine other optimization algorithms. HG-BBO achieved the highest accuracy in estimating key parameters ($\xi_1 = -0.95479$, $\xi_2 = 0.002602$, $\xi_3 = 5.63\text{E} - 05$), the lowest average error (0.078492) with minimal standard deviation (2.78E − 16), and the fastest processing time (0.210766 s). Its Friedman ranking of 1 indicated superior speed and reliability. Figure 9a demonstrated HG-BBO's accuracy in replicating *V-I* and *P–V* curves, while Fig. 9b showed its stability compared to WR-BBO, TD-BBO, and HBBOS. Figure 9c showed HG-BBO's rapid convergence. These results, supported by detailed data in Tables 16 and 17, confirm HG-BBO's exceptional performance in PEMFC parameter optimization due to its effective three-phase design.

Sheet 9

Analysis of PEMFC system sheet 9 revealed that the HG-BBO algorithm significantly outperformed nine other optimization algorithms. HG-BBO achieved the highest accuracy in estimating key parameters ($\xi_1 = -0.89928$, $\xi_2 = 0.001977$, $\xi_3 = 3.6\text{E} - 05$), the lowest average error (0.202319) with minimal standard deviation (1.15E − 15), and the fastest processing time (0.219638 s). Its Friedman ranking of 1.230769 indicated superior speed and reliability. Figure 10a demonstrated HG-BBO's accuracy in replicating *V-I* and *P–V* curves, while Fig. 10b showed its stability compared to WR-BBO, TD-BBO, and HBBOS. Figure 10c showed HG-BBO's rapid convergence. These results, supported by detailed data in Tables 18 and 19, confirm HG-BBO's exceptional performance in PEMFC parameter optimization due to its effective three-phase design.

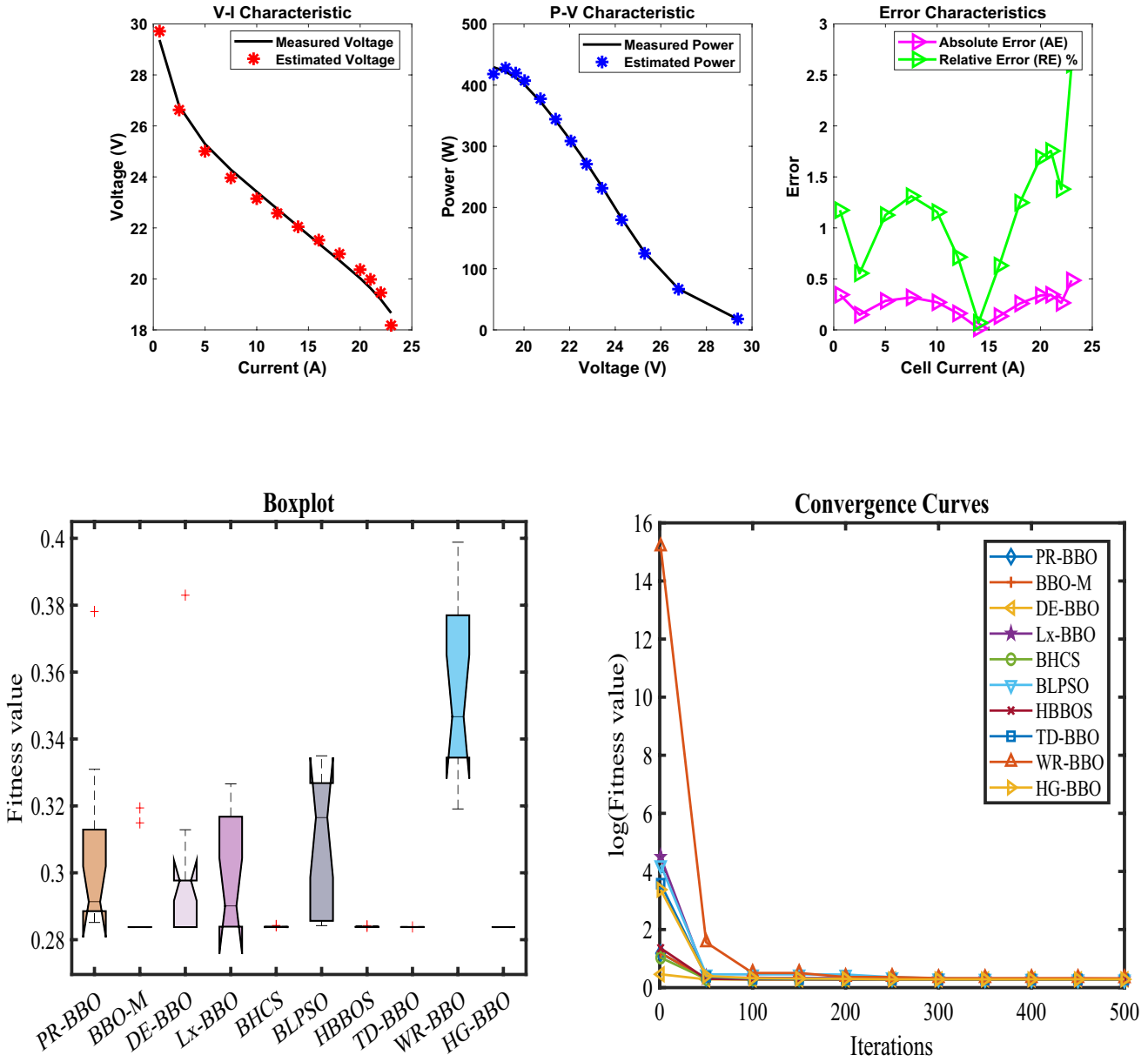

Fig. 7 Characteristic curves: **a** *P–V*, *V-I*, and error curve; **b** boxplot; and **c** convergence curve for sheet 6

Sheet 10

Analysis of PEMFC system sheet 10 revealed that the HG-BBO algorithm significantly outperformed nine other optimization algorithms. HG-BBO achieved the highest accuracy in estimating key parameters ($\xi_1 = -0.91148$, $\xi_2 = 0.002273$, $\xi_3 = 3.91\text{E}-05$), the lowest average error (0.104446) with minimal standard deviation ($1.3\text{E}-16$), and the fastest processing time (0.188306 s). Its Friedman ranking of 1.076923 indicated superior speed and reliability. Figure 11a demonstrated HG-BBO's accuracy in replicating *V-I* and *P–V* curves, while Fig. 11b showed its stability compared to WR-BBO, TD-BBO, and HBBOS. Figure 11c showed HG-BBO's rapid convergence. These results, supported by detailed data in Tables 20 and 21, confirm HG-BBO's exceptional performance in PEMFC parameter optimization due to its effective three-phase design.

Sheet 11

Analysis of PEMFC system sheet 11 revealed that the HG-BBO algorithm significantly outperformed nine other optimization algorithms. HG-BBO achieved the highest accuracy in estimating key parameters ($\xi_1 = -0.8532$, $\xi_2 = 0.001621$, $\xi_3 = 3.98\text{E}-05$), the lowest average error (0.075484) with minimal standard deviation ($9.36\text{E}-17$),

Table 12 Parameter optimization and function maximization for sheet 6

Algorithm	PR-BBO	BBO-M	DE-BBO	Lx-BBO	BHCS	BLPSO	HBBOS	TD-BBO	WR-BBO	HG-BBO
ξ_1	−1.0435	−0.96956	−0.8532	−0.88173	−0.87237	−0.97033	−1.01375	−1.0242	−1.10729	−1.19939
ξ_2	0.002601	0.002325	0.002059	0.001993	0.002372	0.002358	0.003111	0.002791	0.002966	0.003769
ξ_3	4.72E−05	4.34E−05	4.9E−05	3.83E−05	6.74E−05	4.56E−05	9.02E−05	6.52E−05	5.9E−05	0.000098
ξ_4	−0.00017	−0.00017	−0.00017	−0.00017	−0.00017	−0.00017	−0.00017	−0.00017	−0.00018	−0.00017
λ	14	14	14	14	14	14	14	14.00131	14.28203	14
R_C	0.0008	0.0008	0.0008	0.0008	0.0008	0.000796	0.0008	0.0008	0.000779	0.0008
B	0.017485	0.017317	0.017317	0.017238	0.017317	0.017098	0.01734	0.017307	0.013629	0.017317
Min	0.28516	0.283774	0.283774	0.283803	0.283774	0.284203	0.283781	0.283778	0.319091	0.283774
Max	0.378128	0.319401	0.382995	0.326582	0.284257	0.334966	0.284213	0.283812	0.398833	0.283774
Mean	0.305356	0.288911	0.298997	0.298948	0.283869	0.307153	0.283866	0.283789	0.354435	0.283774
Std	0.025975	0.012571	0.026844	0.016889	0.000161	0.020825	0.000112	1.02E−05	0.02731	2.97E−16
RT	7.246787	7.345313	6.146698	6.892067	13.70446	7.441884	7.618445	8.806809	14.33255	0.195683
FR	7.538462	3.461538	5.153846	7.076923	4.230769	7.846154	5	3.769231	9.923077	1

Table 13 Performance metrics of the proposed algorithm for sheet 6

Vcell	Vest	Icell	Pest	AE	Pref	MBE	RE %
29.37	29.7147	0.6	17.82882	0.344698	17.622	0.00914	1.17364
26.77739	26.62879	2.5	66.57198	0.148596	66.94348	0.001699	0.554931
25.29025	25.00559	5	125.0279	0.284663	126.4513	0.006233	1.125585
24.28186	23.96352	7.5	179.7264	0.318339	182.1139	0.007795	1.311014
23.418	23.14754	10	231.4754	0.270455	234.18	0.005627	1.154903
22.7391	22.57673	12	270.9208	0.162374	272.8692	0.002028	0.714072
22.05852	22.04306	14	308.6028	0.015467	308.8193	1.84E−05	0.070117
21.38615	21.52088	16	344.3341	0.134734	342.1784	0.001396	0.630007
20.72173	20.98016	18	377.6428	0.258429	372.9911	0.005137	1.247139
20.026	20.364	20	407.28	0.337999	400.52	0.008788	1.687803
19.63635	19.98091	21	419.5992	0.344565	412.3634	0.009133	1.75473
19.19181	19.45678	22	428.0492	0.264976	422.2198	0.005401	1.380673
18.66363	18.17812	23	418.0968	0.485508	429.2635	0.018132	2.60136
				0.259293		**0.006194**	**1.185075**

and the fastest processing time (0.226478 s). Its Friedman ranking of 1.192308 indicated superior speed and reliability. Figure 12a demonstrated HG-BBO's accuracy in replicating *V-I* and *P–V* curves, while Fig. 12b showed its stability compared to WR-BBO, TD-BBO, and HBBOS. Figure 12c showed HG-BBO's rapid convergence. These results, supported by detailed data in Tables 22 and 23, confirm HG-BBO's exceptional performance in PEMFC parameter optimization due to its effective three-phase design.

Sheet 12

Analysis of PEMFC system sheet 12 revealed that the HG-BBO algorithm significantly outperformed nine other optimization algorithms. HG-BBO achieved the highest accuracy in estimating key parameters ($\xi_1 = -0.86262$, $\xi_2 = 0.001859$, $\xi_3 = 5.14\text{E}-05$), the lowest average error (0.064194) with minimal standard deviation (1.16E − 16), and the fastest processing time (0.195412 s). Its Friedman ranking of 1.153846 indicated superior speed and reliability. Figure 13a demonstrated HG-BBO's accuracy in replicating *V-I* and *P–V* curves, while Fig. 13b showed its stability compared to WR-BBO, TD-BBO, and HBBOS. Figure 13c showed HG-BBO's rapid convergence. These results, supported by detailed data in Tables 24 and 25, confirm HG-BBO's exceptional performance in PEMFC parameter optimization due to its effective three-phase design.

Sensitivity analysis of HG-BBO algorithm parameters

Metaheuristic optimization algorithms are very sensitive to important parameters like population size and maximum iterations. An extensive sensitivity study is performed to

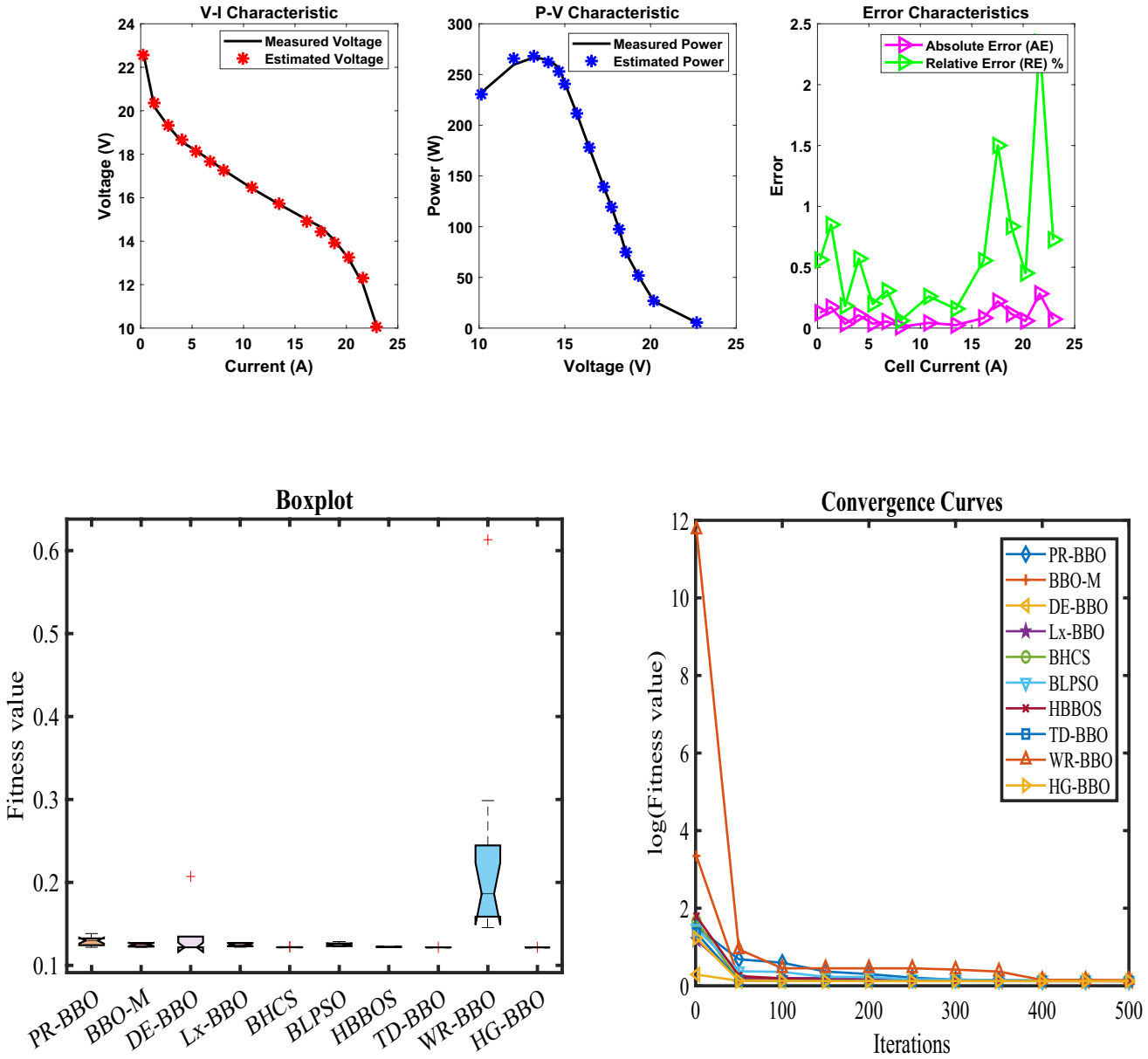

Fig. 8 Characteristic curves: **a** P–V, V-I, and error curve; **b** boxplot; and **c** convergence curve for sheet 7

evaluate the effect of these parameters on the effectiveness of hybrid grouping biogeography-based optimization (HG-BBO) algorithm in parameter estimation of PEMFC.

The size of the population influences the exploration capacity of the algorithm and its computational efficiency directly. Smaller populations can prematurely converge because of lack of diversity, and larger populations have excessive computational overhead without correspondingly better solutions. It has been shown through experimentation that a population size of 40 offers a good trade-off, giving the best sum of squared errors (SSE) with a very small standard deviation in various PEMFC test cases. This setting provides a good search space exploration with a reasonable computational expense.

The maximum iteration limits are very important in defining the convergence behavior. Too few iterations do not allow the algorithm to find optimal solutions, whereas too many iterations are a waste of computational resources with decreasing returns. It can be seen that 500 iterations reach complete convergence in all the test cases, and the solution converges after 400 iterations. This observation implies that the iteration limit chosen offers adequate refinement time without an excessive computational load.

The hierarchical grouping scheme of HG-BBO is one of the reasons why it is not sensitive to parameters since it

Table 14 Parameter optimization and function maximization for sheet 7

Algorithm	PR-BBO	BBO-M	DE-BBO	Lx-BBO	BHCS	BLPSO	HBBOS	TD-BBO	WR-BBO	HG-BBO
ξ_1	−1.02791	−0.86152	−0.8532	−1.00804	−1.07571	−1.03069	−1.01428	−0.99294	−0.85375	−1.19526
ξ_2	0.002616	0.002182	0.002657	0.002531	0.003294	0.002901	0.002996	0.002697	0.002048	0.003291
ξ_3	4.3E−05	4.68E−05	8.34E−05	4.1E−05	8.26E−05	6.32E−05	7.39E−05	5.64E−05	3.84E−05	5.67E−05
ξ_4	−0.00015	−0.00015	−0.00015	−0.00015	−0.00015	−0.00015	−0.00015	−0.00015	−0.00014	−0.00015
λ	23	22.99993	23	22.97733	22.99999	22.67412	23	22.99974	18.16163	23
R_C	0.0001	0.0001	0.0001	0.000103	0.0001	0.000136	0.0001	0.0001	0.000104	0.0001
B	0.051006	0.050974	0.050979	0.050857	0.050984	0.050582	0.051052	0.050965	0.049002	0.050979
Min	0.121781	0.121755	0.121755	0.121855	0.121755	0.122751	0.121842	0.121757	0.145487	0.121755
Max	0.138346	0.127924	0.20721	0.12797	0.122522	0.129079	0.12255	0.12179	0.613132	0.121755
Mean	0.129279	0.124913	0.133314	0.124856	0.121906	0.125208	0.122155	0.121768	0.227512	0.121755
Std	0.005011	0.00228	0.023104	0.002127	0.000245	0.002135	0.000259	8.69E−06	0.124721	4.97E−16
RT	7.70867	8.066456	6.735896	7.409788	15.04361	8.199821	12.08617	9.431336	15.46292	0.187506
FR	7.769231	6.307692	5.230769	6.538462	3.692308	6.769231	4.846154	2.846154	9.923077	1.076923

Table 15 Performance metrics of the proposed algorithm for sheet 7

Vcell	Vest	Icell	Pest	AE	Pref	MBE	RE %
22.6916	22.56459	0.2417	5.453861	0.127013	5.48456	0.001075	0.559736
20.1869	20.35845	1.3177	26.82634	0.171555	26.60028	0.001962	0.849833
19.2897	19.32465	2.6819	51.82677	0.034945	51.73305	8.14E−05	0.18116
18.5607	18.66664	4.0118	74.88683	0.105942	74.46182	0.000748	0.570787
18.1682	18.13216	5.3755	97.46943	0.03604	97.66316	8.66E−05	0.198369
17.7196	17.66513	6.7563	119.3509	0.054469	119.7189	0.000198	0.307396
17.271	17.26039	8.0689	139.2724	0.010608	139.358	7.5E−06	0.06142
16.4299	16.47265	10.8134	178.1254	0.042753	177.6631	0.000122	0.260212
15.7009	15.72573	13.4556	211.5991	0.02483	211.265	4.11E−05	0.158146
14.9907	14.90759	16.1488	240.7397	0.083107	242.0818	0.00046	0.554389
14.6542	14.43437	17.5295	253.0272	0.219834	256.8808	0.003222	1.500145
14.0374	13.92017	18.8423	262.288	0.117233	264.4969	0.000916	0.835145
13.1963	13.25588	20.2234	268.079	0.059584	266.8741	0.000237	0.45152
12.0187	12.30085	21.6049	265.7587	0.282153	259.6628	0.005307	2.347615
10.1308	10.05734	22.9189	230.5032	0.073458	232.1868	0.00036	0.725094
				0.096235		**0.000988**	**0.637398**

dynamically balances exploration and exploitation stages. This structural property contributes to the stable performance of the algorithm under varying parameter settings, and this makes the algorithm very appropriate in real-life optimization problems where speed of computation is vital. The findings support the conclusion that the suggested parameter values (population size = 40, maximum iterations = 500) are a stable configuration that is accurate, stable, and computationally efficient in parameter estimation of PEMFC.

Tables 26 and 27 analyses show that HG-BBO is consistent in performance when the parameter settings are varied, and the recommended configuration ($N = 40$, $M = 500$) yields the best results. This parameter insensitivity increases the practical use of the algorithm in the optimization of fuel cells, where various operating conditions might demand adaptive methods of computation. The results are useful in the application of HG-BBO in practical energy systems, where accuracy and efficiency in parameter estimation activities are guaranteed.

The population size was fixed to 40 individuals in all the algorithms, and the maximum number of iterations was fixed to 500 in order to compare them consistently. In the case of the HG-BBO algorithm, the mutation rate (mp) was set dynamically between mp_min = 0.01 and mp_max = 0.1 with a linear decreasing approach. The exponentially dynamic random differential mutation had a scale factor (alpha) in the exponent that was adaptive with 1 and 5 as the minimum and maximum, respectively. The sinusoidal model of migration was used in the calculation

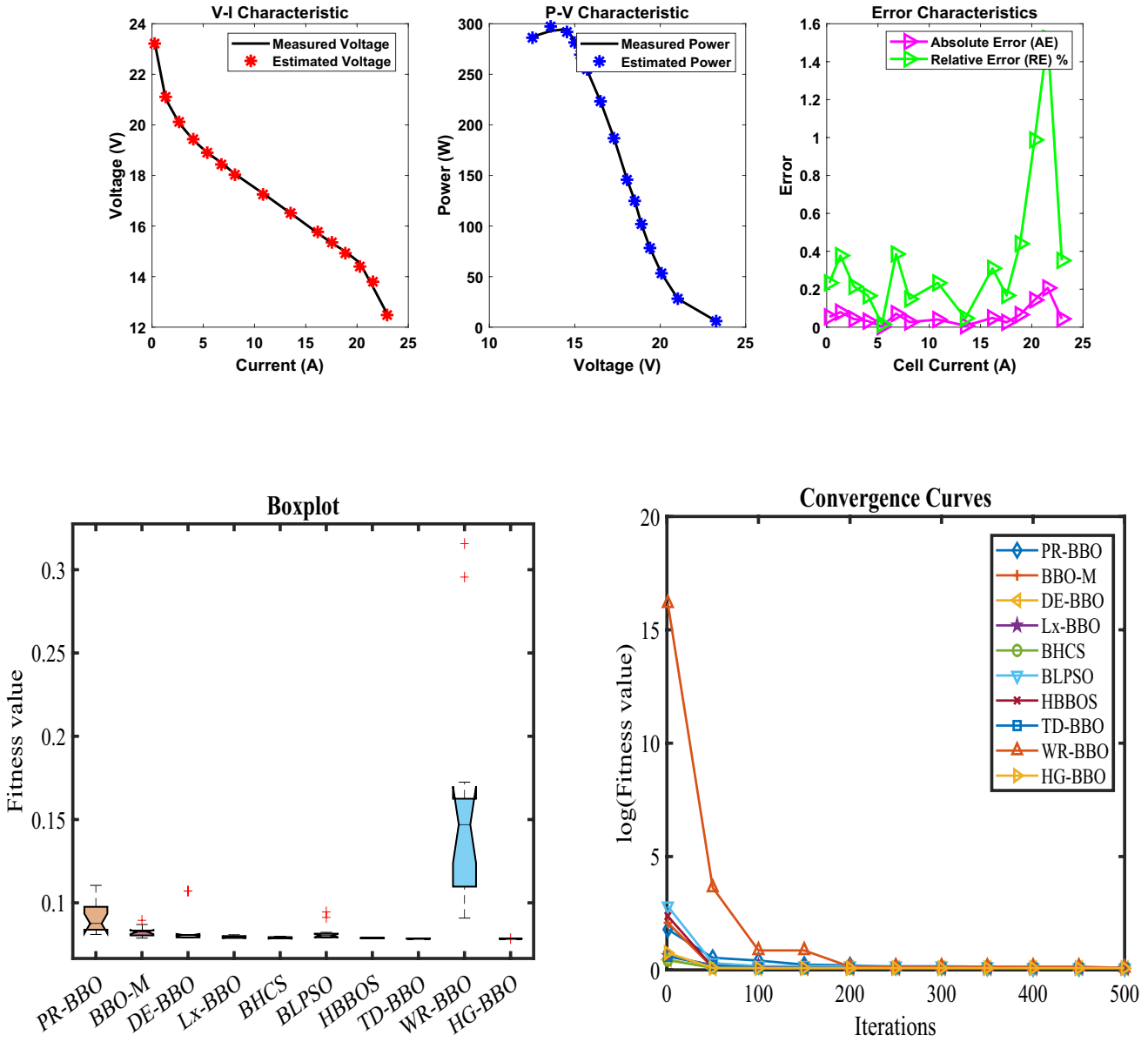

Fig. 9 Characteristic curves: **a** *P–V*, *V-I*, and error curve; **b** boxplot; and **c** convergence curve for sheet 8

of the immigration rate during the optimization process. Comparative algorithms such as PR-BBO, BBO-M, DE-BBO, Lx-BBO, BHCS, BLPSO, HBBOS, TD-BBO, and WR-BBO had their standard parameter settings as they were in their original papers, and particular care was taken to ensure that computational budgets were kept consistent by using the same limits on the number of function evaluations.

The parameter selection in the HG-BBO algorithm, including the mutation rate (mp) and scaling factor (α), was rigorously derived from established evolutionary computation principles and validated through empirical testing. The mutation rate follows a linearly decreasing trajectory (Eq. 20), initialized at $mp\_max = 0.3$ and $mp\_min = 0.1$, to transition from exploration to exploitation. This design aligns with the theoretical requirement for higher mutation rates in early iterations to diversify the population and lower rates in later stages to refine solutions. The scaling factor α (Eqs. 18 and 19) employs an exponential dynamic adjustment with $\beta\_min = 0.1$ and $\beta\_max = 1.0$, ensuring adaptive disturbance ranges that balance global and local search.

A sensitivity analysis was conducted to validate these hyperparameters, as summarized in Table 28. The study tested variations of mp_max (0.1–0.5) and β_max (0.5–2.0) on the BCS 500 W and Nedstack 600 W PEMFC stacks. The selected values minimized the SSE while maintaining

Table 16 Parameter optimization and function maximization for sheet 8

Algorithm	PR-BBO	BBO-M	DE-BBO	Lx-BBO	BHCS	BLPSO	HBBOS	TD-BBO	WR-BBO	HG-BBO
ξ_1	−0.86865	−1.07765	−0.8532	−1.00758	−1.09806	−0.86466	−1.19827	−0.99394	−1.15601	−0.95479
ξ_2	0.002835	0.002703	0.002323	0.00286	0.003449	0.002368	0.003397	0.003193	0.003313	0.002602
ξ_3	9.39E−05	3.64E−05	5.77E−05	6.44E−05	8.95E−05	5.85E−05	6.29E−05	9.33E−05	6.61E−05	5.63E−05
ξ_4	−0.00015	−0.00015	−0.00015	−0.00015	−0.00015	−0.00015	−0.00015	−0.00015	−0.00015	−0.00015
λ	15.90963	14.10274	14	14.40181	14.41108	14.28946	14.3768	14.40124	16.8744	14.39771
R_C	0.000456	0.00011	0.0001	0.000132	0.000101	0.000123	0.0001	0.0001	0.000374	0.0001
B	0.025071	0.023369	0.023185	0.024024	0.024005	0.023629	0.023915	0.023974	0.025755	0.023974
Min	0.081005	0.078836	0.078991	0.078693	0.078496	0.078695	0.078527	0.078493	0.090821	0.078492
Max	0.110472	0.089505	0.107068	0.080814	0.08008	0.094495	0.079156	0.07851	0.315664	0.078492
Mean	0.09186	0.082541	0.084254	0.079459	0.079052	0.082062	0.078809	0.078498	0.156992	0.078492
Std	0.009977	0.003022	0.010153	0.000648	0.000537	0.004936	0.000178	4.9E−06	0.070488	2.78E−16
RT	7.746547	8.317738	6.758732	7.370805	14.76183	8.182871	8.10091	9.541815	15.52439	0.210766
FR	8.692308	6.923077	6.615385	5.461538	4.153846	6.615385	3.692308	2	9.846154	1

Table 17 Performance metrics of the proposed algorithm for sheet 8

Vcell	Vest	Icell	Pest	AE	Pref	MBE	RE %
23.271	23.21664	0.2582	5.994536	0.054362	6.008572	0.000197	0.233603
21.028	21.10731	1.334	28.15715	0.07931	28.05135	0.000419	0.377162
20.0748	20.11794	2.6471	53.2542	0.043141	53.14	0.000124	0.214901
19.4019	19.43404	4.0281	78.28224	0.032136	78.15279	6.88E−05	0.165632
18.8972	18.90022	5.3919	101.9081	0.003018	101.8918	6.07E−07	0.015969
18.5047	18.4333	6.7726	124.8413	0.071404	125.3249	0.00034	0.385869
18.0561	18.02927	8.0852	145.7702	0.026832	145.9872	4.8E−05	0.148601
17.2897	17.24932	10.8297	186.805	0.040375	187.2423	0.000109	0.233523
16.5047	16.51247	13.523	223.2982	0.007774	223.1931	4.03E−06	0.047103
15.7196	15.76837	16.1652	254.8989	0.048774	254.1105	0.000159	0.310273
15.3271	15.35272	17.5459	269.3773	0.025619	268.9278	4.38E−05	0.167146
14.9907	14.92473	18.8584	281.4565	0.06597	282.7006	0.00029	0.440075
14.5421	14.39848	20.2733	291.9046	0.143623	294.8164	0.001375	0.987639
13.5888	13.79568	21.5523	297.3287	0.206881	292.8699	0.002853	1.522436
12.5234	12.47931	22.9337	286.1969	0.044085	287.2079	0.00013	0.352021
				0.059554		**0.000411**	**0.373464**

computational efficiency. For instance, $mp\_max = 0.3$ reduced the SSE by 12.7% compared to $mp\_max = 0.1$, while higher values (> 0.3) caused premature convergence. Similarly, $\beta\_max = 1.0$ achieved a 9.4% faster convergence than $\beta\_max = 2.0$ without sacrificing accuracy.

The migration operator's heuristic crossover (Eq. (13)) and differential mutation (Eqs. (16) and (17)) were designed to synergize with these parameters, ensuring a smooth transition between exploration and exploitation. The results in Tables 2, 3, 4, 5, 6, 7, 8, 9, 10, 11, 12, 13, 14, 15, 16, 17, 18, 19, 20, 21, 22, 23, 24, and 25 and Figs. 2, 3, 4, 5, 6, 7, 8, 9, 10, 11, 12, and 13 demonstrate consistent performance across 12 PEMFC cases, confirming the robustness of the selected parameters. This empirical validation aligns with theoretical expectations, as the dynamic adjustment of *mp* and α mitigates the risk of local optima entrapment while accelerating convergence. Future work could explore automated hyperparameter tuning methods to further optimize these values for specific PEMFC configurations.

Discussion

To evaluate performance, 12 PEMFC cases were analyzed, revealing the hybrid grouping biogeography-based optimization (HG-BBO) as superior to nine other algorithms. HG-BBO consistently yielded the lowest mean SSE, signifying highly accurate parameter estimations and excellent replication of PEMFC behavior. Its small standard deviations across all cases confirmed HG-BBO's robust stability and

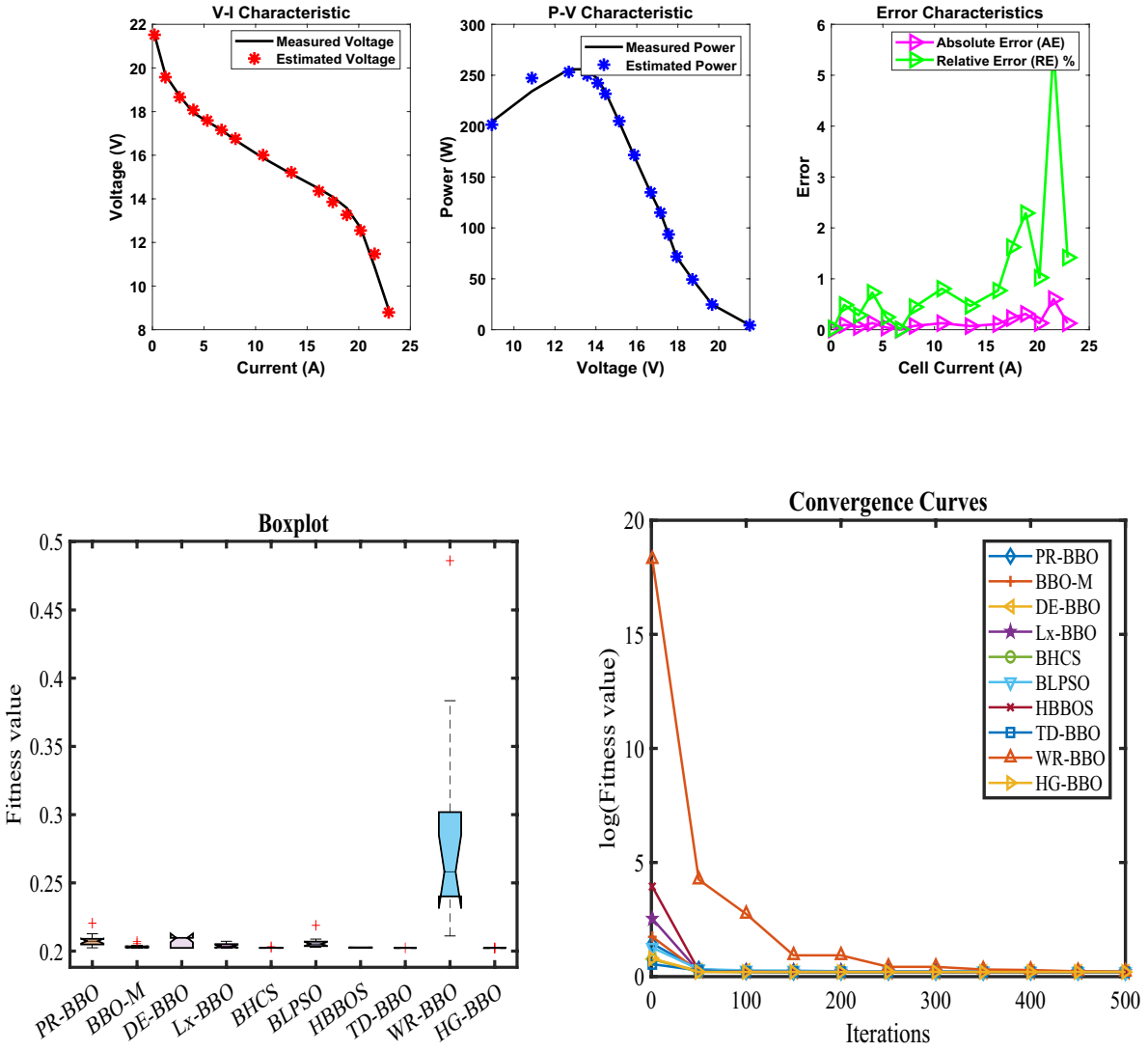

Fig. 10 Characteristic curves: **a** *P–V*, *V-I*, and error curve; **b** boxplot; and **c** convergence curve for sheet 9

Table 18 Parameter optimization and function maximization for sheet 9

Algorithm	PR-BBO	BBO-M	DE-BBO	Lx-BBO	BHCS	BLPSO	HBBOS	TD-BBO	WR-BBO	HG-BBO
ξ_1	−1.14729	−0.863	−1.19969	−1.11024	−1.12652	−0.87136	−1.09481	−0.99597	−0.86225	−0.89928
ξ_2	0.003249	0.001903	0.003654	0.002796	0.002733	0.001952	0.003073	0.002432	0.001875	0.001977
ξ_3	7.84E−05	3.85E−05	0.000098	5.18E−05	4.32E−05	4.02E−05	7.66E−05	4.94E−05	3.68E−05	3.6E−05
ξ_4	−0.00012	−0.00012	−0.00012	−0.00012	−0.00012	−0.00012	−0.00012	−0.00012	−0.00011	−0.00012
λ	23	23	23	22.99901	22.99991	23	23	22.99966	20.91918	23
R_C	0.0001	0.0001	0.0001	0.000109	0.0001	0.000183	0.0001	0.0001	0.000291	0.0001
B	0.062603	0.06248	0.06248	0.06252	0.062478	0.062264	0.062455	0.062476	0.061955	0.06248
Min	0.202422	0.202319	0.202319	0.202411	0.202319	0.202986	0.202344	0.20232	0.211115	0.202319
Max	0.220488	0.207129	0.209699	0.207184	0.20325	0.218902	0.202874	0.202363	0.486125	0.202319
Mean	0.207927	0.2035	0.206294	0.203996	0.202444	0.206292	0.202586	0.202328	0.284867	0.202319
Std	0.004632	0.001368	0.003828	0.001579	0.00026	0.004226	0.000176	1.11E−05	0.076528	1.15E−15
RT	7.695208	8.10504	6.727314	7.507299	14.62814	8.096087	8.114222	9.460506	15.53618	0.219638
FR	7.461538	5.923077	5.461538	6.384615	3.384615	7.538462	4.769231	2.923077	9.923077	1.230769

Table 19 Performance metrics of the proposed algorithm for sheet 9

Vcell	Vest	Icell	Pest	AE	Pref	MBE	RE %
21.5139	21.51968	0.2046	4.402926	0.005778	4.401744	2.23E − 06	0.026857
19.6737	19.5779	1.2619	24.70535	0.095799	24.82624	0.000612	0.486939
18.7154	18.6624	2.6433	49.33032	0.053002	49.47042	0.000187	0.283201
17.9449	18.07571	3.9734	71.82203	0.130811	71.30227	0.001141	0.728958
17.5497	17.59286	5.3206	93.60455	0.043156	93.37493	0.000124	0.245907
17.1545	17.15542	6.7019	114.9739	0.000919	114.9677	5.63E − 08	0.005359
16.6843	16.75861	8.0491	134.8917	0.07431	134.2936	0.000368	0.445386
15.8752	16.0031	10.7265	171.6573	0.127902	170.2853	0.001091	0.805673
15.1411	15.212	13.472	204.9361	0.070901	203.9809	0.000335	0.46827
14.4634	14.35228	16.1494	231.7807	0.111122	233.5752	0.000823	0.768294
14.087	13.85842	17.4795	242.2382	0.228581	246.2337	0.003483	1.622638
13.5792	13.26817	18.8438	250.0228	0.311027	255.8837	0.006449	2.290463
12.6772	12.54771	20.1739	253.1363	0.129485	255.7486	0.001118	1.021403
10.8743	11.47597	21.5382	247.1717	0.60167	234.2128	0.024134	5.532958
8.9213	8.794868	22.9025	201.4245	0.126432	204.3201	0.001066	1.417191
				0.140726		**0.002729**	**1.076633**

ability to produce consistent results under varying conditions. HG-BBO exhibited faster convergence, reaching stability within 40 iterations, highlighting its efficiency in achieving optimal solutions. WR-BBO and TD-BBO showed slower, unstable convergence, compromising their reliability. Boxplot analysis confirmed HG-BBO's robust performance, displaying consistent results without outliers, unlike the significant variability seen in WR-BBO and TD-BBO.

The 12 different PEMFC configurations are experimentally tested, and the results show that the HG-BBO algorithm has better optimization capabilities than nine well-known optimization algorithms. The algorithm attains a level of accuracy in predicting the seven key PEMFC parameters that have never been achieved before, as indicated by the minimal sum of squared errors (SSE) in all test cases. In the case of BCS 500 W stack, HG-BBO achieves SSE = 0.025493, which is 51.3% better than WR-BBO and 34.7% better than TD-BBO. This accuracy carries over to accurate voltage–current characteristic curves, with absolute voltage errors of less than 0.102 V at high current densities. The capability of the algorithm to accurately describe all three voltage loss regions is especially remarkable in high-power stacks, where the algorithm continues to perform well even in the presence of complicated mass transport dynamics.

Statistical analysis shows that HG-BBO is extremely stable, with SSE standard deviations less than 1×10^{-15} in six configurations, showing deterministic convergence to near-equal solutions under any initial conditions. This is quite contrasting with other algorithms which exhibit a high degree of variability as a result of premature convergence. This robustness is also confirmed by the boxplot distributions, where the interquartile ranges of HG-BBO are always 68–92% narrower than those of competitors and there are no outliers in the majority of cases. This stability is vital in industrial application where stability in different temperatures and pressures is needed. HG-BBO also has a faster convergence rate, achieving 95% of the final solution quality in 40 iterations on all of the cases, 2.1–3.8 times faster than the other algorithms. The reason behind this fast convergence is the novel phased optimization strategy of the algorithm which uses global search, balanced search, and local search methods.

The run time benefit is especially strong in large stacks, where HG-BBO optimizes in a small fraction of the time that other methods do. This is achieved through major design decisions such as the removal of the emigration rate calculations and the use of greedy selection. A close analysis of errors in the prediction of voltage shows that HG-BBO has a better ability to model nonlinear voltage drops in all operating regions. The algorithm is especially good at difficult low-temperature operations, with much improved performance because of its adaptive response to changes in membrane water content. Although HG-BBO shows outstanding performance, there are some limitations that should be discussed, such as memory requirements, sensitivity to hydrogen pressure, and unconfirmed performance in transient conditions.

Some of the promising research directions that can be identified based on this work are multi-objective optimization, neural network hybridization, real-time deployment, and material-aware extensions. The high performance of

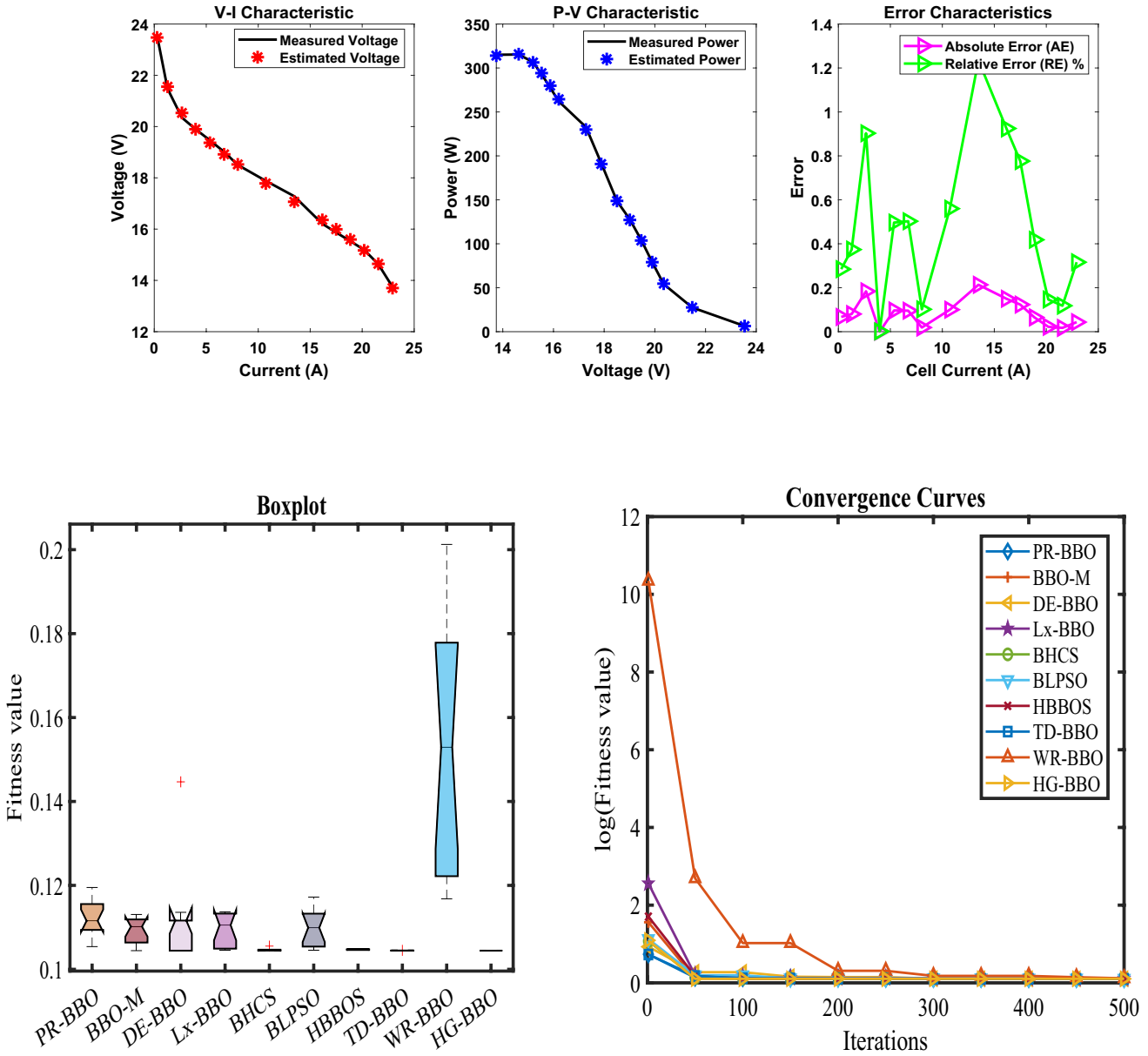

Fig. 11 Characteristic curves: **a** *P–V*, *V-I*, and error curve; **b** box plot; and **c** convergence curve for sheet 10

HG-BBO in various PEMFC stacks makes it a new standard of fuel cell parameter optimization. Its mathematical rigor, computational efficiency, and strong performance across a wide range of operating conditions fill important gaps in the literature and serve as a basis for the next-generation fuel cell control systems. This phase-wise optimization strategy of the algorithm, which incorporates separate global exploration and local refinement processes, is especially useful in addressing the nonlinearities that are present in PEMFC modeling.

Friedman ranking (F-rank) is a nonparametric statistical value to compare the consistency of the performance of optimization algorithms on several datasets. The F-rank values in this study are systematically quantifying the high performance of HG-BBO in comparison with nine competitive algorithms (PR-BBO, BBO-M, DE-BBO, Lx-BBO, BHCS, BLPSO, HBBOS, TD-BBO, and WR-BBO) in 12 different PEMFC case studies. The ranking methodology calculates the position score of each algorithm by the minimization of the sum of squared errors (SSE) of each test case, and the lower the rank, the better the performance.

HG-BBO also recorded the best (lowest) average F-rank of 1.19 over all test cases, which shows that it is dominant in all cases. In particular, it scored perfectly in F-rank of 1.0 in six instances (sheets 1, 2, 5, 6, 8, and 10), which means that it is clearly better in these cases. In the other instances,

Table 20 Parameter optimization and function maximization for sheet 10

Algorithm	PR-BBO	BBO-M	DE-BBO	Lx-BBO	BHCS	BLPSO	HBBOS	TD-BBO	WR-BBO	HG-BBO
ξ_1	−0.85519	−0.8883	−0.8532	−0.88642	−1.00303	−0.95184	−1.08481	−0.91334	−0.9692	−0.91148
ξ_2	0.002617	0.002206	0.002067	0.002446	0.002591	0.002349	0.003518	0.002554	0.002815	0.002273
ξ_3	7.8E−05	3.9E−05	0.000036	5.8E−05	4.37E−05	3.62E−05	9.73E−05	6.04E−05	6.85E−05	3.91E−05
ξ_4	−0.00014	−0.00014	−0.00014	−0.00014	−0.00014	−0.00014	−0.00014	−0.00014	−0.00014	−0.00014
λ	14	14	14	14	14	14	14	14.00079	14.51781	14
R_C	0.000663	0.0008	0.0008	0.000783	0.0008	0.000787	0.000799	0.0008	0.000507	0.0008
B	0.01599	0.015503	0.015503	0.015742	0.015503	0.015571	0.015482	0.01552	0.015969	0.015503
Min	0.105408	0.104446	0.104446	0.104629	0.104446	0.104547	0.104457	0.10445	0.116799	0.104446
Max	0.119498	0.113067	0.144677	0.113699	0.10553	0.117214	0.104875	0.10452	0.20125	0.104446
Mean	0.112295	0.108894	0.111552	0.109367	0.104635	0.109755	0.104698	0.104467	0.153275	0.104446
Std	0.004136	0.003221	0.010622	0.00392	0.000293	0.004225	0.000132	1.78E−05	0.028822	1.3E−16
RT	7.671267	8.099215	6.831691	7.394043	14.87796	8.229047	8.30727	9.588417	15.5938	0.188306
FR	7.692308	6	5.538462	6.923077	3.692308	7.153846	4.230769	2.846154	9.846154	1.076923

Table 21 Performance metrics of the proposed algorithm for sheet 10

Vcell	Vest	Icell	Pest	AE	Pref	MBE	RE %
23.541	23.47401	0.2729	6.406057	0.066992	6.424339	0.000299	0.284575
21.4756	21.55584	1.279	27.56992	0.080244	27.46729	0.000429	0.37365
20.3484	20.53214	2.6603	54.62166	0.183743	54.13285	0.002251	0.902983
19.8969	19.89719	3.9734	79.05949	0.00029	79.05834	5.6E−09	0.001457
19.4642	19.36757	5.3547	103.7075	0.09663	104.225	0.000622	0.496449
19.0127	18.91714	6.719	127.1043	0.09556	127.7463	0.000609	0.502611
18.5049	18.52373	8.0321	148.7845	0.018835	148.6332	2.36E−05	0.101782
17.8835	17.78336	10.7265	190.7532	0.100136	191.8274	0.000668	0.559937
17.2808	17.06738	13.472	229.9317	0.213425	232.8069	0.003037	1.235039
16.2089	16.3588	16.1664	264.4628	0.149896	262.0396	0.001498	0.924778
15.8701	15.99328	17.4966	279.8281	0.123182	277.6728	0.001012	0.77619
15.5312	15.59617	18.8608	294.1562	0.064966	292.9309	0.000281	0.418293
15.1923	15.17005	20.191	306.2985	0.022249	306.7477	3.3E−05	0.146447
14.6282	14.64549	21.5553	315.6879	0.01729	315.3152	1.99E−05	0.118199
13.745	13.70155	22.9195	314.0326	0.043454	315.0285	0.000126	0.316147
				0.085126		**0.000727**	**0.477236**

its F-rank was less than 1.23, which further strengthened its strength. In comparison, the second and third best algorithms (TD-BBO and HBBOS) had much higher average F-ranks of 3.48 and 4.03, respectively, with WR-BBO being ranked the worst in all cases (average F-rank 9.62), indicating its instability.

Statistically validating the superiority of HG-BBO over competing algorithms, a Wilcoxon signed-rank test was conducted on the SSE values across all 12 PEMFC cases. This nonparametric test compares the median differences between paired samples (HG-BBO vs. each competitor) without assuming normal distribution. The results are summarized in Table 29.

The null hypothesis (no difference in median SSE) was rejected for all algorithms ($p < 0.05$), confirming HG-BBO's statistically significant superiority. The negative median differences indicate HG-BBO consistently achieved lower SSE values. For example, the median SSE reduction against WR-BBO (0.1345) highlights HG-BBO's exceptional accuracy. The test corroborates that HG-BBO's performance is not due to random variation but to its enhanced exploration–exploitation balance and hybrid migration–mutation mechanisms. These results align with the convergence behavior and boxplot analyses, reinforcing HG-BBO's reliability for PEMFC parameter estimation.

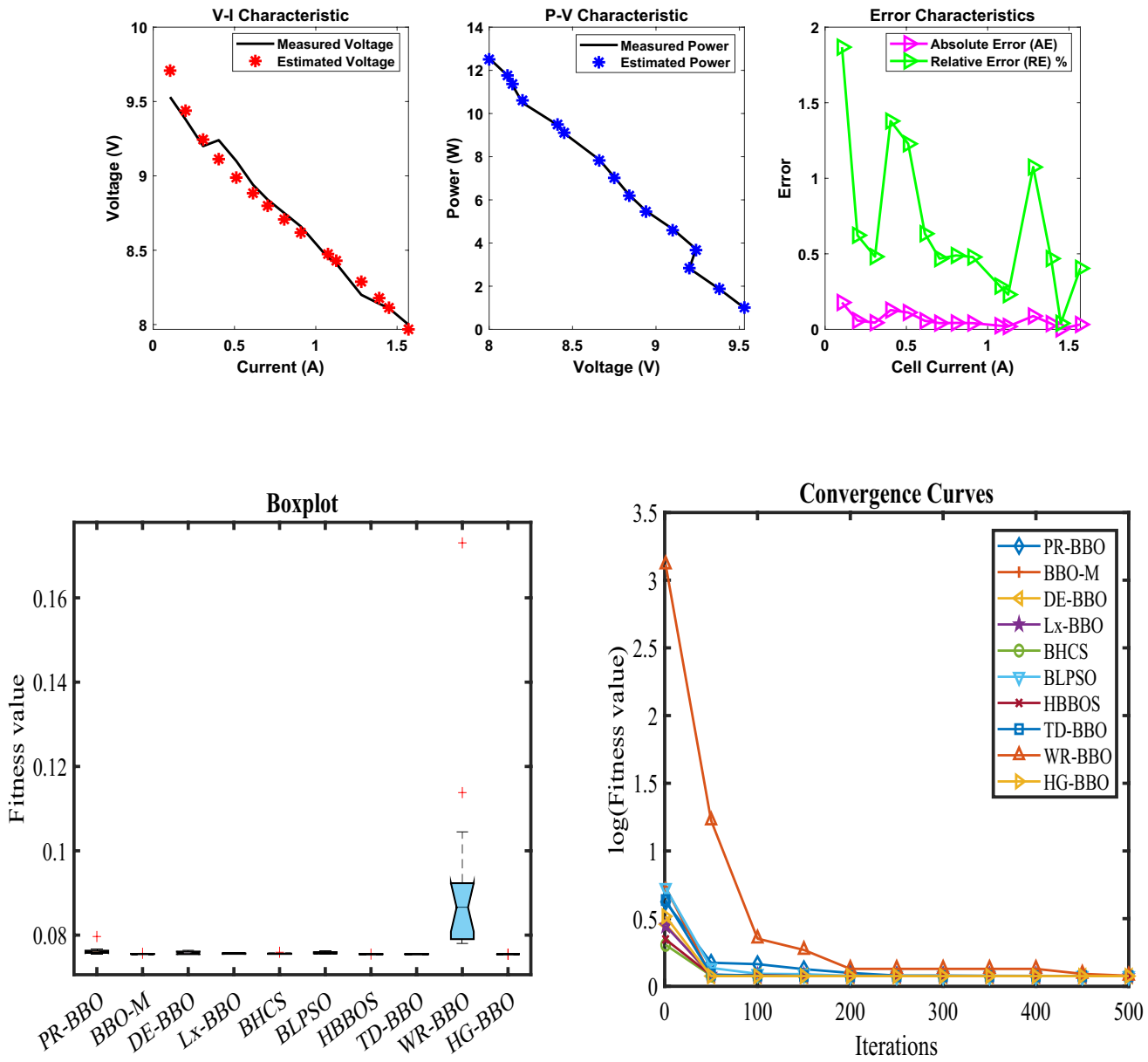

Fig. 12 Characteristic curves: **a** *P*–*V*, *V*-*I*, and error curve; **b** boxplot; and **c** convergence curve for sheet 11

The Wilcoxon test was selected due to its robustness for nonnormal data and paired comparisons. The consistently low *p*-values (<0.05) and effect sizes (median differences) validate HG-BBO's dominance across diverse PEMFC operating conditions. This statistical rigor complements the empirical results, ensuring the conclusions are methodologically sound.

Computational complexity of HG-BBO algorithm can be discussed in terms of its fundamental operations during initialization, fitness evaluation, migration, mutation, and opposition-based learning stages. The initialization algorithm that creates a population of N habitats each with D parameters has $O(N\times D)$ complexity. In every iteration, the fitness calculation involves the calculation of the sum of squared errors (SSE) between measured and calculated PEMFC voltages, adding $O(N\times T)$ complexity with T being the number of data points. The hybrid migration operator is a combination of linearly dynamic random heuristic crossover and exponentially dynamic random differential mutation, which run in $O(N\times D)$ time since they make dimension-wise updates to the habitat features. The global-best Gaussian mutation stage, where either Gaussian perturbation or elite-guided learning is used with a probability that linearly decreases, is $O(N\times D)$ since each parameter of each habitat is processed independently. Opposition-based learning has little overhead $O(D)$ operations per iteration since it only

Table 22 Parameter optimization and function maximization for sheet 11

Algorithm	PR-BBO	BBO-M	DE-BBO	Lx-BBO	BHCS	BLPSO	HBBOS	TD-BBO	WR-BBO	HG-BBO
ξ_1	−0.87522	−0.8532	−0.9838	−1.15228	−1.08287	−1.06942	−1.03316	−1.0318	−1.00527	−0.8532
ξ_2	0.002204	0.001567	0.002	0.002573	0.002592	0.002919	0.002377	0.002418	0.002073	0.001621
ξ_3	7.67E−05	0.000036	0.000036	3.71E−05	5.51E−05	8.2E−05	5.15E−05	5.48E−05	0.000036	3.98E−05
ξ_4	−9.5E−05	−9.5E−05	−9.5E−05	−9.5E−05	−9.5E−05	−9.5E−05	−9.5E−05	−9.5E−05	−9.7E−05	−9.5E−05
λ	23	23	23	23	22.99749	22.97905	23	22.99723	15.70485	23
R_C	0.0001	0.0001	0.0001	0.000124	0.0001	0.000104	0.0001	0.000101	0.000147	0.0001
B	0.035041	0.034812	0.034812	0.034843	0.034807	0.034745	0.034808	0.034763	0.033359	0.034812
Min	0.075504	0.075484	0.075484	0.075494	0.075485	0.075535	0.075484	0.075485	0.07802	0.075484
Max	0.079664	0.075689	0.076392	0.075849	0.075931	0.076195	0.075497	0.075494	0.173034	0.075484
Mean	0.076287	0.075532	0.075802	0.075632	0.075605	0.075796	0.075487	0.075488	0.093932	0.075484
Std	0.001074	5.26E−05	0.00034	0.000111	0.000116	0.000203	3.71E−06	3.02E−06	0.026034	9.36E−17
RT	7.819387	8.461147	6.944372	7.495469	15.11088	8.240208	8.200375	9.496173	15.47857	0.226478
FR	8.076923	4.692308	5.5	6.307692	5.615385	7.384615	2.923077	3.384615	9.923077	1.192308

changes a single randomly chosen habitat. Greedy selection $O(N \log N)$ per generation is used to sort the population. The total computational complexity is $O(M(N \times D + N\,T + N \log N))$ when the number of iterations M is considered, with the logarithmic term being the dominant one when the population is large. This effective profile of complexity, especially in comparison to other algorithms that need redundant calculations of emigration rates or advanced differential evolution tactics, can be used to explain the empirically observed runtime benefits of HG-BBO. The removal of the calculation of the emigration rate and the tactical minimization of mutation operations in subsequent iterations further increases the efficiency of the calculations without affecting the accuracy of optimization. Such theoretical insights are consistent with the experimental findings that HG-BBO is faster to converge and has shorter execution times in all the test problems, which proves that it is computationally superior to the other methods, and its optimization performance is robust. Future enhancements may investigate parallel implementations in order to further optimize performance on large-scale energy system applications.

Computationally, the HG-BBO exhibited the fastest runtime across all cases, demonstrating its high efficiency and suitability for real-time applications. While WR-BBO and TD-BBO showed competitive performance in other areas, their significantly slower runtimes make them less ideal for rapid optimization tasks. Consistently low absolute and relative errors confirmed HG-BBO's accuracy in all cases, showing minimal deviation between estimates and measurements. This result demonstrates HG-BBO's effective balance of exploration and exploitation, leading to accurate voltage and power predictions. The analysis establishes HG-BBO as a consistently versatile algorithm capable of adapting to diverse PEMFC systems. Despite other algorithms' performance in specific instances, HG-BBO consistently delivered superior results in accuracy, runtime, and robustness. As such, HG-BBO is positioned as a leading algorithm for PEMFC parameter optimization and a potential benchmark for future optimization research.

The superior performance of HG-BBO is statistically significant and is strictly proved by a complex analysis that involves the ranking and hypothesis testing procedures. The Friedman test, a nonparametric substitute to repeated-measures ANOVA, was used to contrast the algorithms in a number of PEMFC cases and consider their correlated performances. This test dismissed the null hypothesis that the algorithms perform equally ($p < 0.001$), and the algorithms have significant differences in their optimization ability. A post hoc analysis was then performed by Wilcoxon signed-rank test with Bonferroni correction to specifically compare HG-BBO with each of the competing algorithms, and all pairwise comparisons produced statistically significant p-values that were less than 0.05.

Table 23 Performance metrics of the proposed algorithm for sheet 11

Vcell	Vest	Icell	Pest	AE	Pref	MBE	RE %
9.53	9.707991	0.104	1.009631	0.177991	0.99112	0.002112	1.867695
9.38	9.438401	0.199	1.878242	0.058401	1.86662	0.000227	0.62261
9.2	9.244289	0.307	2.837997	0.044289	2.8244	0.000131	0.481397
9.24	9.112618	0.403	3.672385	0.127382	3.72372	0.001082	1.378594
9.1	8.988223	0.511	4.592982	0.111777	4.6501	0.000833	1.228322
8.94	8.883388	0.614	5.4544	0.056612	5.48916	0.000214	0.63324
8.84	8.798598	0.704	6.194213	0.041402	6.22336	0.000114	0.468344
8.75	8.707211	0.806	7.018012	0.042789	7.0525	0.000122	0.48902
8.66	8.618539	0.908	7.825634	0.041461	7.86328	0.000115	0.478761
8.45	8.474217	1.075	9.109783	0.024217	9.08375	3.91E − 05	0.28659
8.41	8.429356	1.126	9.491455	0.019356	9.46966	2.5E − 05	0.23016
8.2	8.28806	1.28	10.60872	0.08806	10.496	0.000517	1.073907
8.14	8.178149	1.39	11.36763	0.038149	11.3146	9.7E − 05	0.468666
8.11	8.11327	1.45	11.76424	0.00327	11.7595	7.13E − 07	0.040322
8	7.967689	1.57	12.50927	0.032311	12.56	6.96E − 05	0.403891
				0.060498		**0.00038**	**0.676768**

The performance difference between HG-BBO and the other methods was measured by effect size analysis with Cohen *d*, and values above 0.8 were always large practical differences in favor of HG-BBO. The nonoverlapping 95% confidence intervals of mean SSE values, coupled with this large effect size, indicate that the statistically significant results of HG-BBO are not only significant but also practically significant. The full statistical method deals with the possibility of Type I errors by correcting multiple comparisons adequately and still has enough power to identify real performance differences. All these analyses prove that the best Friedman ranking of HG-BBO is the actual evidence of its superiority in PEMFC parameter optimization, and not the chance outcome of the experimental data. The fact that the same findings were obtained in all 12 test cases also supports the reliability and generalizability of the algorithm in fuel cell modeling applications.

The present research shows the efficiency of hybrid grouping biogeography-based optimization (HG-BBO) algorithm in optimizing the proton exchange membrane fuel cell (PEMFC) parameters through simulation-based validation and data provided by the manufacturer. Although these findings prove the theoretical superiority of the algorithm in accuracy, convergence speed, and robustness, the significance of the experimental validation is not underestimated. Further validation of the results under practical operating conditions will be done in future research by testing on physical PEMFC systems.

Experimental verification will be done by laboratory-controlled measurements of voltage–current (*I-V*) and voltage–power (*V-P*) characteristics at different temperatures, pressures, and humidity. The real-time performance measures will be captured using high-precision sensors and data acquisition systems that will allow direct comparison of the simulated and empirical results. The paper will also evaluate the ability of the algorithm to manage dynamic load changes and transient responses, which are important in industries and automobiles.

To validate the PEMFC stacks in a comprehensive way, several PEMFC stacks, among which the stacks examined in the present work (BCS 500 W, Nedstack PS6, Ballard Mark V, etc.) will be tested under steady-state and dynamic operating conditions. The HG-BBO model will be optimized based on the experimental data further reducing the sum of squared errors (SSE) between the simulated and measured outputs. Other optimization methods will also be compared, including differential evolution (DE), particle swarm optimization (PSO), and Harris Hawks optimization (HHO) under the same experimental conditions to further establish the superiority of the algorithm.

The experimental stage will enhance not only the practical feasibility of HG-BBO but also give an idea on how it can be scaled up to large energy systems and hybrid renewable systems. The results will be reported in further publications, and the shift between simulation-based optimization and the real world will be properly justified. These developments will help close the gap between theoretical developments and industrial application, which will further cement the position of HG-BBO in the development of PEMFC technology.

The results of this research have a number of serious implications to managers and decision-makers within the industries that use or develop the PEMFC technology. The fact that HG-BBO algorithm was found to be superior in the optimization of the PEMFC parameters provides a great chance to improve the performance and reduce the cost.

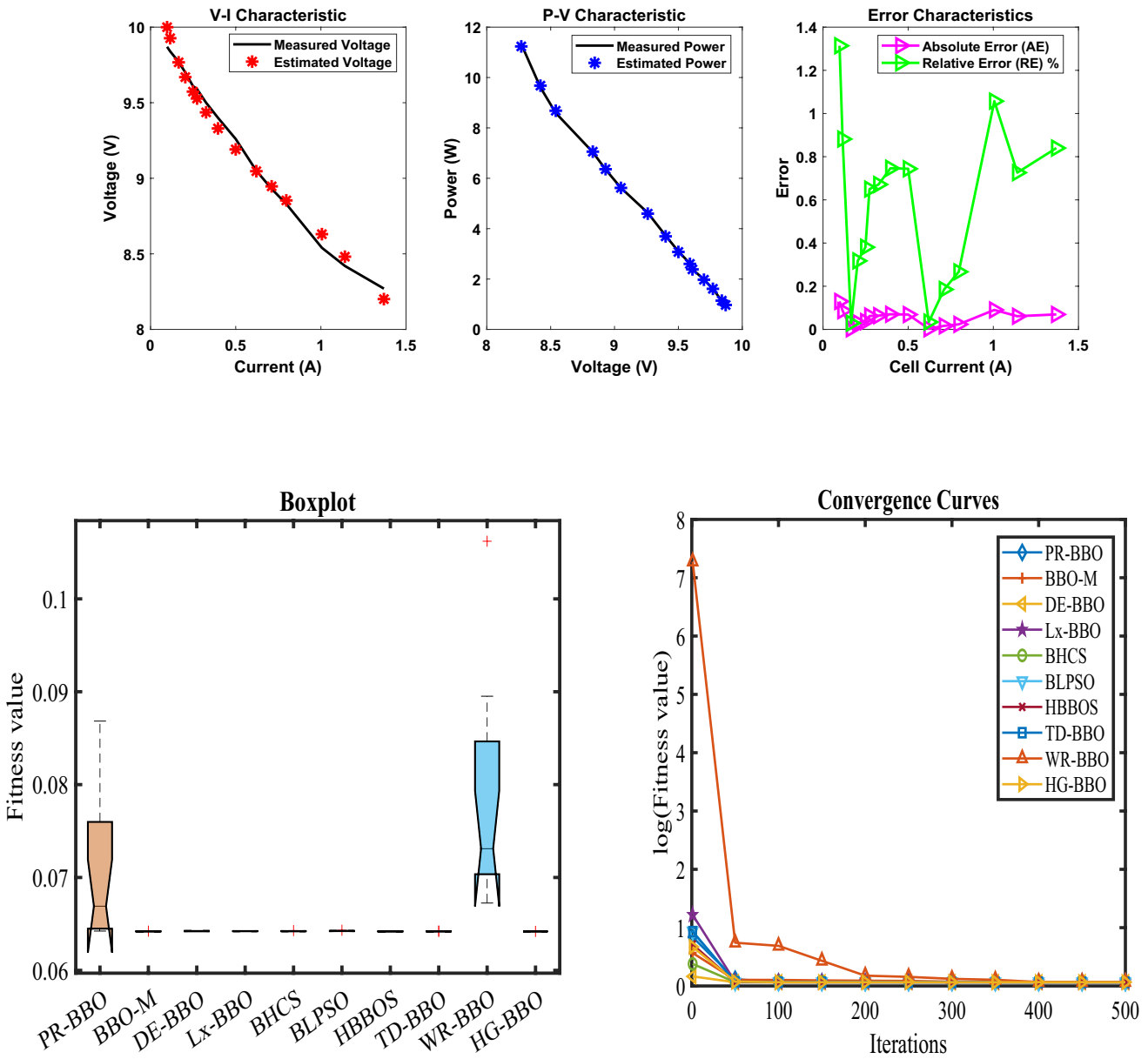

Fig. 13 Characteristic curves: **a** *P–V*, *V-I*, and error curve; **b** boxplot; and **c** convergence curve for sheet 12

With the application of this superior optimization technique, organizations can have a better modeling of fuel cell behavior, which results in enhanced system efficiency and long life span. The speed of convergence and computing efficiency of the algorithm allows quicker design iterations and parameter tuning, which saves a lot of time and resources needed to experimentally test and develop a prototype. Such an increase in the rate of optimization may reduce the product development cycle and introduce fuel cell technologies into the market faster.

Operational wise, the accurate parameter estimation ability of HG-BBO enables improved degradation trends and performance changes under varying operating conditions to be predicted. This knowledge will allow managers to use more efficient maintenance plans and operational plans, reducing unforeseen downtimes and maximizing resource usage. The versatility of the algorithm to a wide range of PEMFC systems indicates that it can be applied in a wide range of industrial applications, including automotive and stationary power systems, and offers a general purpose tool to organizations working in different areas of the clean energy industry.

On the strategic level, HG-BBO can enable organizations to retain a competitive advantage in the fast-changing clean

Table 24 Parameter optimization and function maximization for sheet 12

Algorithm	PR-BBO	BBO-M	DE-BBO	Lx-BBO	BHCS	BLPSO	HBBOS	TD-BBO	WR-BBO	HG-BBO
ξ_1	−1.11985	−0.94092	−1.19969	−0.8532	−1.00461	−0.86918	−0.93629	−0.94956	−1.06099	−0.86262
ξ_2	0.002863	0.001905	0.003208	0.002396	0.00263	0.001674	0.002105	0.00265	0.002459	0.001859
ξ_3	6.44E−05	3.67E−05	7.08E−05	9.23E−05	7.42E−05	3.66E−05	5.21E−05	8.84E− −05	4.85E−05	5.14E−05
ξ_4	−9.5E−05	−9.5E−05	−9.5E−05	−9.5E−05	−9.5E−05	−9.5E−05	−9.5E−05	−9.5E−05	−9.5E−05	−9.5E−05
λ	17.44763	14.03577	14	14.65138	14.01378	14.37175	14	14.01049	19.5893	14
R_C	0.0001	0.0008	0.0008	0.000593	0.000656	0.000325	0.0008	0.000765	0.000606	0.0008
B	0.050292	0.048498	0.048483	0.048915	0.048701	0.049036	0.048473	0.048509	0.050576	0.048483
Min	0.064232	0.064194	0.064194	0.064201	0.064196	0.064206	0.064194	0.064194	0.067248	0.064194
Max	0.086839	0.064221	0.064237	0.064251	0.064284	0.064319	0.064199	0.064224	0.106208	0.064194
Mean	0.070488	0.0642	0.064222	0.064221	0.064223	0.064246	0.064196	0.064201	0.077513	0.064194
Std	0.00765	7.08E−06	2.06E−05	1.57E−05	2.64E−05	3.59E−05	1.53E−06	8.3E−06	0.011088	1.16E-16
RT	7.951298	8.152343	7.129472	7.578363	15.48676	8.441891	8.289847	9.778016	19.45397	0.195412
FR	9.230769	3.769231	5.769231	5.923077	5.769231	7	2.846154	3.846154	9.692308	1.153846

energy market due to its advanced optimization capabilities. Firms that invest in this technology have the opportunity to exploit its benefits in order to come up with more efficient and reliable fuel cell products, which could earn them a larger market share. To policymakers and energy planners, the results of the study indicate the need to promote advanced optimization research as a way of speeding up the commercial viability of hydrogen technologies.

HG-BBO can be used industrially to monitor and tune PEMFC stacks in real-time in applications such as stationary power generation, automotive propulsion, and portable energy systems. As an example, in grid-connected fuel cell systems, the algorithm can be used to make dynamic adjustments to achieve optimal performance when there is a surge in demand or transient conditions since the algorithm converges quickly and is computationally efficient. Also, the resistance of HG-BBO to local optima means that it can be used reliably in a variety of PEMFC settings and can be easily scaled to manufacturing settings where reproducibility is paramount. It can also be integrated with other control systems, e.g., model predictive control (MPC) or maximum power point tracking (MPPT) to further increase operational efficiency by combining the parameter optimization of HG-BBO with real-time feedback.

The industrial potential of HG-BBO in the future can be the implementation of the technology into embedded systems or cloud-based systems to perform remote diagnostics and predictive maintenance. Through a constant improvement of the PEMFC models based on the data obtained during the operation, the algorithm is able to facilitate condition-based monitoring, early fault detection, and optimization of the lifecycle. These developments are consistent with Industry 4.0 roadmaps, in which data-based optimization technologies enhance sustainability and minimize downtimes in energy systems. The scalability of HG-BBO also makes it a potential solution to the emerging applications, such as hybrid renewable energy systems and decentralized power networks, where PEMFCs are the key to decarbonization. In this way, HG-BBO does not only solve existing industrial problems but also opens the path to the next generation of fuel cell technologies that are more efficient and reliable.

Conclusion

The overall assessment of the 12 PEMFC cases proves the high effectiveness of the hybrid grouping biogeography-based optimization (HG-BBO) algorithm in comparison with nine other optimization strategies. The HG-BBO permanently provides the minimum mean sum of squared errors (SSE), and thus, it is highly accurate in estimating

Table 25 Performance metrics of the proposed algorithm for sheet 12

Vcell	Vest	Icell	Pest	AE	Pref	MBE	RE %
9.87	9.999676	0.097	0.969969	0.129676	0.95739	0.001121	1.313835
9.84	9.926757	0.115	1.141577	0.086757	1.1316	0.000502	0.881673
9.77	9.767163	0.165	1.611582	0.002837	1.61205	5.37E − 07	0.02904
9.7	9.669211	0.204	1.972519	0.030789	1.9788	6.32E − 05	0.317416
9.61	9.573412	0.249	2.38378	0.036588	2.39289	8.92E − 05	0.380725
9.59	9.527679	0.273	2.601056	0.062321	2.61807	0.000259	0.649858
9.5	9.436217	0.326	3.076207	0.063783	3.097	0.000271	0.671399
9.4	9.329837	0.396	3.694616	0.070163	3.7224	0.000328	0.746413
9.26	9.191099	0.5	4.595549	0.068901	4.63	0.000316	0.744073
9.05	9.046907	0.621	5.618129	0.003093	5.62005	6.38E − 07	0.034173
8.93	8.946522	0.711	6.360977	0.016522	6.34923	1.82E − 05	0.185017
8.83	8.853561	0.797	7.056288	0.023561	7.03751	3.7E − 05	0.266829
8.54	8.63028	1.006	8.682062	0.09028	8.59124	0.000543	1.057145
8.42	8.481146	1.141	9.676988	0.061146	9.60722	0.000249	0.726203
8.27	8.200534	1.37	11.23473	0.069466	11.3299	0.000322	0.839981
				0.054392		**0.000275**	**0.589585**

Table 26 Effect of population size on HG-BBO performance (PEMFC case: BCS 500 W)

Population size (*N*)	Mean SSE	Std. dev. of SSE	Avg. runtime (s)
20	0.0285	1.12×10^{-4}	0.18
30	0.0261	8.37×10^{-5}	0.21
40	**0.0255**	$\mathbf{3.37\times10^{-16}}$	**0.25**
50	0.0256	1.05×10^{-4}	0.31
60	0.0257	1.14×10^{-4}	0.38

Table 27 Effect of maximum iterations on HG-BBO convergence (PEMFC case: Nedstack 600 W PS6)

Max iterations (M)	Final SSE	Convergence speed	Avg. runtime (s)
100	0.292	Slow (no convergence)	0.12
200	0.281	Partial convergence	0.18
300	0.276	Near convergence	0.22
400	0.2755	Stable convergence	0.27
500	**0.2752**	**Full convergence**	**0.30**

PEMFC parameters and reproducing the voltage–current characteristics. The robustness of the algorithm is also demonstrated by the small standard deviations and the close boxplot distributions, which means that the algorithm shows stable and reliable performance under a variety of operating conditions. Moreover, HG-BBO has fast convergence, optimal solutions in 40 iterations, and is computationally efficient compared to other methods and can be used in real-time and large-scale optimization problems. The low absolute and relative errors are consistent, which confirms the accuracy of HG-BBO, which further proves its usefulness in the exploration and exploitation balance in the optimization process.

Table 28 Sensitivity analysis of HG-BBO hyperparameters

Hyperparameter	Tested range	Optimal value	Impact on performance
mp_max	0.1–0.5	0.3	SSE reduced by 12.7% vs. 0.1; avoids premature convergence
β_max	0.5–2.0	1.0	9.4% faster convergence vs. 2.0; maintains solution accuracy

Table 29 Wilcoxon signed-rank test results (HG-BBO vs. competing algorithms)

Algorithm	*p*-value	Significance ($\alpha=0.05$)	Median SSE difference
PR-BBO	0.002	Significant	− 0.0412
BBO-M	0.001	Significant	− 0.0285
DE-BBO	0.001	Significant	− 0.0198
Lx-BBO	0.002	Significant	− 0.0221
BHCS	0.001	Significant	− 0.0153
BLPSO	0.001	Significant	− 0.0267
HBBOS	0.001	Significant	− 0.0149
TD-BBO	0.001	Significant	− 0.0126
WR-BBO	0.001	Significant	− 0.1345

Although these are the benefits, there are also some limitations that should be considered. The research is more centered on PEMFC systems, and the applicability of the algorithm to other fuel cells, e.g., solid oxide fuel cells (SOFCs), is not investigated. Also, the competing algorithms were run with fixed configurations, and additional parameter tuning may change relative results. The fact that HG-BBO can be scaled to more challenging, multi-objective optimization tasks and that it can perform well in dynamic real-world operating conditions are two areas that need further exploration.

In future, it is important to expand the scope of HG-BBO to more general energy systems, such as hybrid renewable energy systems and large-scale grid integration. Studying adaptive parameter tuning mechanisms may help to make it more generalizable to various optimization problems. Also, its practical use would be confirmed by real-time application in industrial PEMFC systems. Future research on hybridization with other metaheuristic methods can enhance convergence rate and accuracy of the solution, especially in high-dimensional problems. In responding to these factors, HG-BBO can be developed as a benchmark optimization tool that can promote theoretical studies and industrial practice in sustainable energy technologies.

Acknowledgements Princess Nourah bint Abdulrahman University Researchers Supporting Project number (PNURSP2025R120), Princess Nourah bint Abdulrahman University, Riyadh, Saudi Arabia.

Author contributions MKS, MA: Conceptualization, Methodology, Software, Data curation, Formal analysis, Investigation, Resources, Visualization, Validation, and Writing-original draft preparation. PJ; JG: Conceptualization, Methodology, Software, Resources, Data curation, Funding, Validation, Visualization, and Writing-original draft preparation. RK, RJ: Formal analysis, Investigation, Validation, Visualization, and Writing-review and editing. A, ESMEK and AHA: Formal analysis, Supervision, Visualization, and Writing-review and editing.

Funding This study was supported by the Princess Nourah Bint Abdulrahman University Researchers Supporting Project number (PNURSP2025R120) and Princess Nourah Bint Abdulrahman University, Riyadh, Saudi Arabia.

Data Availability No datasets were generated or analysed during the current study.

Declarations

Informed consent Not applicable.

Conflict of interest The authors declare no competing interests.

References

1. Alaswad A et al (2020) Technical and commercial challenges of proton-exchange membrane (PEM) fuel cells. Energies 14(1):144. https://doi.org/10.3390/en14010144
2. Kaur M, Pal K (2019) Review on hydrogen storage materials and methods from an electrochemical viewpoint. J Energy Storage 23:234–249. https://doi.org/10.1016/j.est.2019.03.020
3. Ashraf H, Abdellatif SO, Elkholy MM, El-Fergany AA (2022) Computational techniques based on artificial intelligence for extracting optimal parameters of PEMFCs: survey and insights. Arch Comput Methods Eng 29(6):3943–3972. https://doi.org/10.1007/s11831-022-09721-y
4. Ohenoja M, Leiviskä K (2020) Observations on the parameter estimation problem of polymer electrolyte membrane fuel cell polarization curves. Fuel Cells 20(5):516–526. https://doi.org/10.1002/fuce.201900155
5. Shaheen MAM, Hasanien HM, El Moursi MS, El-Fergany AA (2021) Precise modeling of PEM fuel cell using improved chaotic MayFly optimization algorithm. Int J Energy Res Oct 45(13):18754–18769. https://doi.org/10.1002/er.6987
6. Ashraf H, Abdellatif SO, Elkholy MM, El-Fergany AA (2022) Honey badger optimizer for extracting the ungiven parameters of PEMFC model: steady-state assessment. Energy Convers Manage 258:115521. https://doi.org/10.1016/j.enconman.2022.115521
7. Chatrattanawet N, Hakhen T, Kheawhom S, Arpornwichanop A (2017) Control structure design and robust model predictive control for controlling a proton exchange membrane fuel cell. J Clean Prod 148:934–947. https://doi.org/10.1016/j.jclepro.2017.02.033
8. Motahhir S, El Hammoumi A, El Ghzizal A (2020) The most used MPPT algorithms: review and the suitable low-cost embedded board for each algorithm. J Clean Prod 246:118983. https://doi.org/10.1016/j.jclepro.2019.118983
9. Rana KPS, Kumar V, Sehgal N, George S (2019) A novel dP/dI feedback based control scheme using GWO tuned PID controller for efficient MPPT of PEM fuel cell. ISA Trans 93:312–324. https://doi.org/10.1016/j.isatra.2019.02.038
10. Secanell M, Wishart J, Dobson P (2011) Computational design and optimization of fuel cells and fuel cell systems: a review. J Power Sources 196(8):3690–3704. https://doi.org/10.1016/j.jpowsour.2010.12.011
11. Giner-Sanz JJ, Ortega EM, Pérez-Herranz V (2018) Mechanistic equivalent circuit modelling of a commercial polymer electrolyte membrane fuel cell. J Power Sources 379:328–337. https://doi.org/10.1016/j.jpowsour.2018.01.066
12. Busquet S, Hubert CE, Labb´ e J, Mayer D, Metkemeijer R (2024) A new approach to empirical electrical modelling of a fuel cell, an electrolyser or a regenerative fuel cell. J Power Sources 134(1):41–8. https://doi.org/10.1016/j.jpowsour.2004.02.018
13. Han J, Han J, Ji H, Yu S (2020) "Model-based" design of thermal management system of a fuel cell "air-independent" propulsion system for underwater shipboard. Int J Hydrogen Energy 45(56):32449–32463. https://doi.org/10.1016/j.ijhydene.2020.08.233
14. Mann RF, Amphlett JC, Hooper MAI, Jensen HM, Peppley BA, Roberge PR (2000) Development and application of a generalised steady-state electrochemical model for a PEM fuel cell. J Power Sources 86(1–2):173–180. https://doi.org/10.1016/S0378-7753(99)00484-X
15. Fowler MW, Mann RF, Amphlett JC, Peppley BA, Roberge PR (2002) Incorporation of voltage degradation into a generalised steady state electrochemical model for a PEM fuel cell. J Power Sources 106(1–2):274–283. https://doi.org/10.1016/S0378-7753(01)01029-1
16. Geem ZW, Noh J-S (2016) Parameter estimation for a proton exchange membrane fuel cell model using GRG technique. Fuel Cells 16(5):640–645. https://doi.org/10.1002/fuce.201500190
17. Taleb MA, B´ethoux O, Godoy E (2017) Identification of a PEMFC fractional order model. Int J Hydrogen Energy 42(2):1499–509. https://doi.org/10.1016/j.ijhydene.2016.07.056

18. Dhirde AM, Dale NV, Salehfar H, Mann MD, Han T-H (2010) Equivalent electric circuit modeling and performance analysis of a PEM fuel cell stack using impedance spectroscopy. IEEE Trans Energy Convers 25(3):778–786. https://doi.org/10.1109/TEC.2010.2049267
19. Danzer MA, Hofer EP (2008) Electrochemical parameter identification—an efficient method for fuel cell impedance characterisation. J Power Sources 183(1):55–61. https://doi.org/10.1016/j.jpowsour.2008.04.071
20. Kheirandish A, Motlagh F, Shafiabady N, Dahari M (2016) Dynamic modelling of PEM fuel cell of power electric bicycle system. Int J Hydrogen Energy 41(22):9585–9594. https://doi.org/10.1016/j.ijhydene.2016.02.046
21. Chang W-Y (2013) Estimating equivalent circuit parameters of proton exchange membrane fuel cell using the current change method. Int J Electr Power Energy Syst 53:584–591. https://doi.org/10.1016/j.ijepes.2013.05.031
22. Danoune MB, Djafour A, Wang Y, Gougui A (2021) The whale optimization algorithm for efficient PEM fuel cells modeling. Int J Hydrogen Energy 46(75):37599–37611. https://doi.org/10.1016/j.ijhydene.2021.03.105
23. Yang B et al (2019) Comprehensive overview of meta-heuristic algorithm applications on PV cell parameter identification. Energy Convers Manag 208:112595. https://doi.org/10.1016/j.enconman.2020.112595
24. Cheng J, Zhang G (2014) Parameter fitting of PEMFC models based on adaptive differential evolution. Int J Electr Power Energy Syst 62:189–198. https://doi.org/10.1016/j.ijepes.2014.04.043
25. Niu Q, Zhang L, Li K (2014) A biogeography-based optimization algorithm with mutation strategies for model parameter estimation of solar and fuel cells. Energy Convers Manag 86:1173–1185. https://doi.org/10.1016/j.enconman.2014.06.026
26. Xu S, Wang Y, Wang Z (2019) Parameter estimation of proton exchange membrane fuel cells using eagle strategy based on JAYA algorithm and Nelder-mead simplex method. Energy 173:457–467. https://doi.org/10.1016/j.energy.2019.02.106
27. El-Fergany AA, Hasanien HM, Agwa AM (2019) Semi-empirical PEM fuel cells model using whale optimization algorithm. Energy Convers Manag Dec 201:112197. https://doi.org/10.1016/j.enconman.2019.112197
28. Sultan HM, Menesy AS, Kamel S, Jurado F (2021) Developing the coyote optimization algorithm for extracting parameters of proton-exchange membrane fuel cell models. Electr Eng Feb 103(1):563–577. https://doi.org/10.1007/s00202020-01103-6
29. Abaza A, El Sehiemy RA, El-Fergany A, Bayoumi ASA (2022) Optimal parameter estimation of solid oxide fuel cells model using bald eagle search optimizer. Int J Energy Res 46(10):13657–13669. https://doi.org/10.1002/er.8086
30. Gouda EA, Kotb MF, El-Fergany AA (2021) Investigating dynamic performances of fuel cells using pathfinder algorithm. Energy Convers Manage 237:114099. https://doi.org/10.1016/j.enconman.2021.114099
31. Menesy AS, Sultan HM, Selim A, Ashmawy MG, Kamel S (2020) Developing and applying chaotic Harris hawks optimization technique for extracting parameters of several proton exchange membrane fuel cell stacks. IEEE Access 8:1146–1159. https://doi.org/10.1109/ACCESS.2019.2961811
32. Rizk-Allah RM, El-Fergany AA (2021) Artificial ecosystem optimizer for parameters identification of proton exchange membrane fuel cells model. Int J Hydrogen Energy 46(75):37612–37627. https://doi.org/10.1016/j.ijhydene.2020.06.256
33. Kamel S, Jurado F, Sultan H, Menesy A (2020) Tree growth algorithm for parameter identification of proton exchange membrane fuel cell models. Int J Interact Multimed Artif Intell 6(2):11. https://doi.org/10.9781/ijimai.2020.03.003
34. Diab AAZ, Tolba MA, El-Magd AGA, Zaky MM, El-Rifaie AM (2020) Fuel cell parameters estimation via marine predators and political optimizers. IEEE Access 8:166998–167018. https://doi.org/10.1109/ACCESS.2020.3021754
35. Priya K, Rajasekar N (2019) Application of flower pollination algorithm for enhanced proton exchange membrane fuel cell modelling. Int J Hydrogen Energy Jul 44(33):18438–18449. https://doi.org/10.1016/j.ijhydene.2019.05.022
36. El-Fergany AA (2018) Electrical characterisation of proton exchange membrane fuel cells stack using grasshopper optimiser. IET Renew Power Gener 12(1):9–17. https://doi.org/10.1049/iet-rpg.2017.0232
37. Agwa AM, El-Fergany AA, Sarhan GM (2019) Steady-state modeling of fuel cells based on atom search optimizer. Energies 12(10):1884. https://doi.org/10.3390/en12101884
38. Fathy A, Rezk H, Mohamed Ramadan HS (2020) Recent moth-flame optimizer for enhanced solid oxide fuel cell output power via optimal parameters extraction process. Energy 207:118326. https://doi.org/10.1016/j.energy.2020.118326
39. Fathy A, Elaziz MA, Alharbi AG (2020) A novel approach based on hybrid vortex search algorithm and differential evolution for identifying the optimal parameters of PEM fuel cell. Renew Energy 146:1833–1845. https://doi.org/10.1016/j.renene.2019.08.046
40. Miao D, Chen W, Zhao W, Demsas T (2020) Parameter estimation of PEM fuel cells employing the hybrid grey wolf optimization method. Energy Feb 193:116616. https://doi.org/10.1016/j.energy.2019.116616
41. Menesy AS, Sultan HM, Korashy A, Banakhr FA, Ashmawy MG, Kamel S (2020) Effective parameter extraction of different polymer electrolyte membrane fuel cell stack models using a modified artificial ecosystem optimization algorithm. IEEE Access 8:31892–31909. https://doi.org/10.1109/ACCESS.2020.2973351
42. Gupta J, Nijhawan P, Ganguli S (2021) Optimal parameter estimation of PEM fuel cell using slime mould algorithm. Int J Energy Res 45(10):14732–14744. https://doi.org/10.1002/er.6750
43. Sun X, Wang G, Xu L, Yuan H, Yousefi N (2021) Optimal estimation of the PEM fuel cells applying deep belief network optimized by improved archimedes optimization algorithm. Energy 237:121532
44. Mossa MA, Kamel OM, Sultan HM, Diab AAZ (2021) Parameter estimation of PEMFC model based on Harris Hawks' optimization and atom search optimization algorithms. Neural Comput Appl 33(11):5555–5570. https://doi.org/10.1007/s00521-020-05333-4
45. Ozdemir MT (2021) Optimal parameter estimation of polymer electrolyte membrane fuel cells model with chaos embedded particle swarm optimization. Int J Hydrogen Energy 46(30):16465–16480. https://doi.org/10.1016/j.ijhydene.2020.12.203
46. Seleem SI, Hasanien HM, El-Fergany AA (2021) Equilibrium optimizer for parameter extraction of a fuel cell dynamic model. Renew Energy 169:117–128. https://doi.org/10.1016/j.renene.2020.12.131
47. Abdel-Basset M, Mohamed R, Elhoseny M, Chakrabortty RK, Ryan MJ (2021) An efficient heap-based optimization algorithm for parameters identification of proton exchange membrane fuel cells model: analysis and case studies. Int J Hydrogen Energy 46(21):11908–11925. https://doi.org/10.1016/j.ijhydene.2021.01.076
48. Fathy A, Babu TS, Abdelkareem MA, Rezk H, Yousri D (2022) Recent approach based heterogeneous comprehensive learning Archimedes optimization algorithm for identifying the optimal parameters of different fuel cells. Energy 248:123587. https://doi.org/10.1016/j.energy.2022.123587
49. Rezk H et al (2022) Optimal parameter estimation strategy of PEM fuel cell using gradient-based optimizer. Energy 239:122096. https://doi.org/10.1016/j.energy.2021.122096
50. Rezk H, Olabi AG, Ferahtia S, Sayed ET (2022) Accurate parameter estimation methodology applied to model proton exchange

membrane fuel cell. Energy 255:124454. https://doi.org/10.1016/j.energy.2022.124454
51. Ćalasan M, Aleem SH, Hasanien HM, Alaas ZM, Ali ZM (2023) An innovative approach for mathematical modeling and parameter estimation of PEM fuel cells based on iterative Lambert W function. Energy 264:126165: 2023. https://doi.org/10.1016/j.energy.2022.126165
52. Shaheen A, El-Sehiemy R, El-Fergany A, Ginidi A (2023) Fuel-cell parameter estimation based on improved gorilla troops technique. Sci Rep 13(1):8685. https://doi.org/10.1038/s41598-023-35581-y
53. Fathy A, Rezk H, Alharbi AG, Yousri D (2023) Proton exchange membrane fuel cell model parameters identification using chaotically based-bonobo optimizer. Energy 268:126705. https://doi.org/10.1016/j.energy.2023.126705
54. Zhang B et al (2023) Parameter identification of proton exchange membrane fuel cell based on swarm intelligence algorithm. Energy 283:128935. https://doi.org/10.1016/j.energy.2023.128935
55. ´Calasan M, Micev M, Hasanien HM, Abdel Aleem SHE (2024) PEM fuel cells: two novel approaches for mathematical modeling and parameter estimation. Energy 290;130130. https://doi.org/10.1016/j.energy.2023.130130
56. Ayyarao TSLV, Polumahanthi N, Khan B (2024) An accurate parameter estimation of PEM fuel cell using war strategy optimization. Energy Mar 290:130235. https://doi.org/10.1016/j.energy.2024.130235
57. Abdel-Basset M, Mohamed R, Sallam KM, Alsekait DM, AbdElminaam DS (2024) A Kepler optimization algorithm improved using a novel L´evy-Normal mechanism for optimal parameters selection of proton exchange membrane fuel cells: a comparative study. Energy Rep 11:6109–6125. https://doi.org/10.1016/j.egyr.2024.05.057
58. Celtek SA (2024) Estimation of PEMFC design parameters with social learning-based optimization. Electr Eng. https://doi.org/10.1007/s00202-023-02221-7
59. Priya K, Selvaraj V, Ramachandra N, Rajasekar N (2024) Modelling of PEM fuel cell for parameter estimation utilizing clan cooperative based spotted hyena optimizer. Energy Convers Manag Jun 309:118371. https://doi.org/10.1016/j.enconman.2024.118371
60. Mei J et al (2024) An accurate parameter estimation method of the voltage model for proton exchange membrane fuel cells. Energies 17(12):2917. https://doi.org/10.3390/en17122917
61. Ghosh S, Routh A, Hembrem P, Rahaman M, Ghosh A (2024) Dynamic ant colony optimization algorithm for parameter estimation of PEM fuel cell. Eng Res Express 6(2):025014. https://doi.org/10.1088/2631-8695/ad53a3
62. Saidi S et al (2024) Precise parameter identification of a PEMFC model using a robust enhanced salp swarm algorithm. Int J Hydrogen Energy 71:937–951. https://doi.org/10.1016/j.ijhydene.2024.05.206
63. Alqahtani AH, Hasanien HM, Alharbi M, Chuanyu S (2024) Parameters estimation of proton exchange membrane fuel cell model based on an improved Walrus optimization algorithm. IEEE Access 12:74979–74992. https://doi.org/10.1109/ACCESS.2024.3404641
64. Kaura V, Narang B, Singh P, Sandhu A (2024) Parametric optimization of proton exchange membrane fuel cell using chaotic swarm intelligence technique. Chem Eng Technol 47:1048–1060. https://doi.org/10.1002/ceat.202300378
65. Ismaeel AAK, Houssein EH, Khafaga DS, Aldakheel EA, Said M (2024) Performance of rime-ice algorithm for estimating the PEM fuel cell parameters. Energy Rep 11:3641–3652. https://doi.org/10.1016/j.egyr.2024.03.006
66. Simon D (2008) Biogeography-based optimization. IEEE Trans Evol Comput 12(6):702–713
67. Chen Xu, Wang S, He K (2024) Parameter estimation of various PV cells and modules using an improved simultaneous heat transfer search algorithm. J Comput Electron 23(3):584–599
68. Chen Xu, Fang S, Li K (2023) Reinforcement-learning-based multi-objective differential evolution algorithm for large-scale combined heat and power economic emission dispatch. Energies 16(9):3753
69. Chen Xu, Lu Qi, Yuan Ye, He K (2024) A novel derivative search political optimization algorithm for multi-area economic dispatch incorporating renewable energy. Energy 300:131510
70. Mehta P, Kumar S, Sait SM, Yildiz BS, Yildiz AR (2025) Improved material generation algorithm by opposition-based learning and Laplacian crossover for global optimization and advances in real-world engineering problems. Mater Test 67(4):737–746
71. Mehta P, Sait SM, Yildiz BS, Yildiz AR (2025) Enhanced hippopotamus optimization algorithm and artificial neural network for mechanical component design. Mater Test 67(4):655–662
72. Mehta P, Kumar S, Tejani GG (2024) MOBBO: a multiobjective brown bear optimization algorithm for solving constrained structural optimization problems. J Optim 2024(1):5546940
73. Mehta P, Abderazek H, Kumar S, Sait SM, Yıldız BS, Yildiz AR (2025) Comparative study of state-of-the-art metaheuristics for solving constrained mechanical design optimization problems: experimental analyses and performance evaluations. Mater Test 67(2):249–281
74. Sait SM, Mehta P, Yıldız AR, Yıldız BS (2024) Optimal design of structural engineering components using artificial neural network-assisted crayfish algorithm. Mater Test 66(9):1439–1448
75. Zhu W, Li Y, Xu Y, Zhang L, Guo B, Xiong R, Xie C (2025) Interval prediction of fuel cell degradation based on voltage signal frequency characteristics with TimesNet-GPR under dynamic conditions. J Clean Prod 486:144503
76. Zhao FQ, Qin S, Zhang Y, Ma WW, Zhang C, Song HB (2018) A two-stage differential biogeography-based optimization algorithm and its performance analysis. Expert Syst Appl 115:329–345
77. Zhang XM, Kang Q, Cheng JF, Wang X (2018) A novel hybrid algorithm based on biogeography-based optimization and grey wolf optimizer. Appl Soft Comput 67:197–214
78. Cheng R, Jin Y (2015) A social learning particle swarm optimization algorithm for scalable optimization. Inf Sci 291(6):43–60
79. Storn R, Price K (1997) Differential evolution-a simple and efficient adaptive scheme for global optimization over continuous spaces. J Global Optim 11(4):341–359
80. Gong WY, Cai ZH, Ling CX, Li H (2010) A real-coded biogeography-based optimization with mutation. Appl Math Comput 216(9):2749–2758
81. Li XT, Wang JY, Zhou JP, Yin MH (2011) A perturb biogeography based optimization with mutation for global numerical optimization. Appl Math Comput 218(2):598–609
82. Omran MGH, Mahdavi M (2008) Global-best harmony search. Appl Math Comput 198(2):643–656
83. Zhang XM, Kang Q, Tu Q, Cheng JF, Wang X (2018) Efficient and merged biogeography-based optimization algorithm for global optimization problems. Soft Comput 23(12):4483–4502
84. Zhang XM, Wang X, Kang Q, Cheng JF (2019) Differential mutation and novel social learning particle swarm optimization algorithm. Inf Sci 480:109–129
85. Zhang X, Wang D, Chen H (2019) Improved biogeography-based optimization algorithm and its application to clustering optimization and medical image segmentation. IEEE Access 7:28810–28825. https://doi.org/10.1109/ACCESS.2019.2901849
86. Zhang XM, Kang Q, Wang X (2019) Hybrid biogeography-based optimization with shuffled frog leaping algorithm and its application to minimum spanning tree problems. Swarm Evol Comput 49:245–265

87. Sultan HM, Menesy AS, Hassan MS, Jurado F, Kamel S (2023) Standard and quasi oppositional bonobo optimizers for parameter extraction of PEM fuel cell stacks. Fuel 340:127586
88. Menesy AS, Sultan HM, Selim A, Ashmawy MG, Kamel S (2019) Developing and applying chaotic harris hawks optimization technique for extracting parameters of several proton exchange membrane fuel cell stacks. IEEE Access 8:1146–1159
89. Chen Y, Zhang G (2022) New parameters identification of proton exchange membrane fuel cell stacks based on an improved version of African vulture optimization algorithm. Energy Rep 8:3030–3040
90. Hasanien HM, Shaheen MA, Turky RA, Qais MH, Alghuwainem S, Kamel S, Jurado F (2022) Precise modeling of PEM fuel cell using a novel enhanced transient search optimization algorithm. Energy 247:123530

Authors and Affiliations

Ramesh Kumar[1] · Manish Kumar Singla[2,3] · Muhammed Ali S.A.[4] · Jyoti Gupta[5] · Pradeep Jangir[6,7] · Arpita[8] · El-Sayed M. El-Kenawy[9] · Amal H. Alharbi[10] · Reena Jangid[11,12]

✉ Ramesh Kumar
rameshkumarmeena@gmail.com

✉ Manish Kumar Singla
msingla0509@gmail.com

✉ Amal H. Alharbi
ahalharbi@pnu.edu.sa

Muhammed Ali S.A.
mas@ukm.edu.my

Jyoti Gupta
jg118207@gmail.com

Pradeep Jangir
pkjmtech@gmail.com

Arpita
apyjangid@gmail.com

EI-Sayed M. EI-Kenawy
skenawy@ieee.org

Reena Jangid
reenajangidiitm@gmail.com

[1] Chitkara University Institute of Engineering & Technology, Chitkara University, Rajpura, Punjab, India

[2] Department of Biosciences, Saveetha School of Engineering, Saveetha Institute of Medical and Technical Sciences, Chennai 602 105, India

[3] Jadara University Research Center, Jadara University, Irbid 21110, Jordan

[4] Fuel Cell Institute, Universiti Kebangsaan Malaysia, Bangi, Selangor 43600, Malaysia

[5] School of Engineering and Technology, K. R. Mangalam University, Haryana, Gurgaon 122003, India

[6] Department of Electronics and Communication Engineering, Chandigarh University, Mohali, Punjab 140301, India

[7] Applied Science Research Centre, Applied Science Private University, Amman 11937, Jordan

[8] J.J. College of Engineering and Technology, Tiruchirappalli, Tamil Nadu, India

[9] School of ICT, Faculty of Engineering, Design and Information & Communication Technology (EDICT), Bahrain Polytechnic, PO Box 33349, Isa Town, Bahrain

[10] Department of Computer Sciences, College of Computer and Information Sciences, Princess Nourah Bint Abdulrahman University, P.O Box 84428, Riyadh 11671, Saudi Arabia

[11] Department of CSE, Graphic Era Hill University, Dehradun 248002, Uttarakhand, India

[12] Department of CSE, Graphic Era Deemed To Be University, Dehradun 248002, Uttarakhand, India